BUYUKER Effect of Sediment Load on the Time Evolution of the Morphology of Confluence MASTER' S THESIS 2023

Republic of Turkey

İzmir Kâtip Çelebi University

Graduate School of Natural and Applied Sciences

Effect of Sediment Load on the Time Evolution of the Morphology of a Large-scale Laboratory Movable-bed Symmetrical Confluence

Department of Civil Engineering

Master's Thesis

Zehra Büyüker

ORCID 0000-0001-9987-0951

Thesis Advisor: Prof. Dr. Gökçen Bombar

January 2023

İZMİR KÂTİP ÇELEBİ ÜNİVERSİTESİ
2010
GRADUATE SCHOOL OF NATURAL AND APPLIED SCIENCES

Effect of Sediment Load on the Time Evolution of the Morphology of a Large-scale Laboratory Movable-bed Symmetrical Confluence

M. Sc. Thesis

Department of Civil Engineering

Zehra Büyüker

ORCID 0000-0001-9987-0951

Thesis Advisor: Prof. Dr. Gökçen Bombar

January, 2023

İZMİR KÂTİP ÇELEBİ ÜNİVERSİTESİ
2010
GRADUATE SCHOOL OF NATURAL AND APPLIED SCIENCES

Büyük Ölçekli Laboratuvar Ortamında Sediment Yükünün Hareketli Tabanlı Simetrik Akarsu Kavşağı Morfolojisinin Zamanla Değişimine Etkisi

Yüksek Lisans Tezi

İnşaat Mühendisliği Anabilim Dalı

Zehra Büyüker

ORCID 0000-0001-9987-0951

Tez Danışmanı: Prof. Dr. Gökçen Bombar

Ocak, 2023

This is to certify that we have read the thesis **Effect of Sediment Load on the Time Evolution of the Morphology of a Large-scale Laboratory Movable-bed Symmetrical Confluence** submitted by **Zehra Büyüker**, and it has been judged to be successful, in scope and in quality, at the defense exam and accepted by our jury as a MASTER'S THESIS.

APPROVED BY:

Advisor: **Prof. Dr. Gökçen Bombar**
İzmir Kâtip Çelebi University

Committee Members:

Prof. Dr. Mehmet Sorgun
İzmir Kâtip Çelebi University

Assoc. Prof. Dr. Ebru Eriş
Ege University

Date of Defense: January 16, 2023

Declaration of Authorship

I, **Zehra Büyüker**, declare that this thesis titled **Effect of Sediment Load on the Time Evolution of the Morphology of a Large-scale Laboratory Movable-bed Symmetrical Confluence** and the work presented in it are my own. I confirm that:

- This work was done wholly or mainly while in candidature for the Master's degree at this university.
- Where any part of this thesis has previously been submitted for a degree or any other qualification at this university or any other institution, this has been clearly stated.
- Where I have consulted the published work of others, this is always clearly attributed.
- Where I have quoted from the work of others, the source is always given. This thesis is entirely my own work, with the exception of such quotations.
- I have acknowledged all major sources of assistance.
- Where the thesis is based on work done by myself jointly with others, I have made clear exactly what was done by others and what I have contributed myself.

Date: 16.01.2023

Effect of Sediment Load on the Time Evolution of the Morphology of a Large-scale Laboratory Movable-bed Symmetrical Confluence

Abstract

Stream confluences are the basic elements of natural drainage networks and the habitat they create has high ecological value. The interaction between the sediment load in the tributaries and the flow is an important factor regulating the junction morphology. It is observed that the sediment and flow from the tributary cause scours and accumulations in places along the main channel, and as a result, changes in the bed topography are observed with time.

In this study, two experiments were carried out on the open channel confluence in İzmir Katip Çelebi University Hydraulics Laboratory, where two symmetrical side tributaries are connected to the main channel at an angle of 90˚. While the flow rate from the tributaries is equal and 20 l/s for both experiments, the amount of sediment loads was set as 0 kg/min and 0.1 kg/min. The flow depth at the downstream of the confluence with the cover at the downstream of the experimental set-up was adjusted to be 5 cm. The same conditions were maintained for three different periods of 3 hours, 9 hours and 15 hours, and at the end of each period, the experiment was stopped to obtain the bed elevations. The erosion and accumulation zones in the confluence where the side tributaries meet were investigated.

The bed morphologies t=3 h were the same for both experiments. While a scour corridor was formed in experiment without sediment feeding, the sediment load from the tributaries prevented to devethe erosion in the tributary mouths in experiment with sediment feeding. The bed elevations in the tributaries were higher with sediment feeding. Depending on the amount of sediment load, larger, higher and wider bank-attached bars were observed at the end of the experiment with sediment

feeding. While no scour hole was formed in experiment without sediment feeding, according to effect of the sediment load, a scour hole was observed at the end of the experiment with sediment feeding.

Keywords: Open channel confluence, sediment transport, morphological structure, sediment load, time

Sediment Yükü Nedeniyle Simetrik Akarsu Kavşağı Taban Morfolojisinin Zamanla Değişiminin Laboratuvar Ortamındaki Büyük Ölçekli Bir Düzenek Üzerinde İncelenmesi

Öz

Akarsu kavşakları doğal drenaj ağlarının temel unsurları olup oluşturdukları habitat yüksek ekolojik değer arz etmektedir. Yan kollardaki sediment yükü ve akım arasındaki etkileşim kavşak morfolojisini düzenleyen önemli bir faktördür. Yan koldan gelen sediment yükü ve debinin ana kanal boyunca yer yer oyulmalara ve yığılmalara sebebiyet verdiği, bunların sonucunda da taban topoğrafyasında zamana bağlı değişimlerin olduğu gözlemlenmektedir.

Bu çalışmada İzmir Kâtip Çelebi Üniversitesi Hidrolik Laboratuvarında bulunan, simetrik iki yan kolun 90˚ açı ile ana kanala bağlandığı açık kanal kavşağı üzerinde iki deney gerçekleştirilmiştir. Yan kollardan gelen debi iki deney için de eşit ve 20 l/s iken sediment besleme miktarları 0 kg/dk (E1)ve 0,1 kg/dk (E2) olarak ayarlanmıştır. Deney düzeneğinin mansabında bulunan kapak ile kavşak mansabında akım derinliği 5 cm olacak şekilde ayarlanmıştır. Aynı koşullar 3 saat, 9 saat ve 15 saat olacak şekilde üç farklı süre boyunca devam ettirilmiş ve her süre sonunda deney dondurularak taban kotları elde edilmiştir. Yan kolların birleştiği kavşak bölgesindeki oyulma ve yığılma bölgeleri incelenmiştir.

t=3 s için iki deneyde taban morfolojisi benzerdi. Sediment beslemesiz deneyde oyulma koridori oluşurken sediment beslemeli deneyde yan koldan gelen sediment beslemesi yan kol ağzında oyulma gelişmesini engellemiştir. Yan kollardaki taban kotları sediment beslemesiyle daha yüksekti. Sediment beslemesinin miktarına bağlı olarak sediment beslemeli deneyin sonunda daha geniş, daha yüksek ve daha uzun birikme bölgesi gözlemlenmiştir. Sediment beslemesiz deneyde oyulma çukuru

oluşmamışken, sediment yüküne bağlı olarak, sediment beslemesi deneyin sonunda oyulma çukuru gözlemlenmiştir.

Anahtar Kelimeler: Açık kanal kavşağı, sediment taşınımı, morfolojik yapı, sediment yükü, zaman

To my family.

Acknowledgment

This thesis was supported by The Scientific and Technological Research Council of Turkey, within the scope of the TUBITAK 122M889 project.

The experiments of this study were carried out on the experimental set-up built within the scope of the "Simetrik Akarsu Kavşaklarında Sediment Yükü Nedeniyle Taban Morfolojisinde Oluşan Değişikliğin Deneysel Olarak İncelenmesi" project numbered 2016-GAP-MUMF-0020.

I would like to thank Prof. Dr. Gökmen Tayfur for allowing the use of ULS-40D supplied by the TUBITAK 119M959 project.

I would like to thank Prof. Dr. Gökçen Bombar for her guidance, support and encouragement throughout the preparation of this thesis.

I am grateful to my family for always supporting me all my life.

I also would like to give my deepest thanks to my husband Necati Büyüker who tried to find a solution to every problem during my graduate education, supported and trusted me endlessly.

Thanks also to the Hakkı Mert Bölceci, Gülhan Eraktülü and Eyüp Dinçer who helped me during the experimens.

Table of Contents

List of Figures

List of Tables

List of Abbreviations and Symbols

ORCID	Open Researcher and Contributor ID
TÜBİTAK	Türkiye Bilimsel ve Teknolojik Araştırma Kurumu

d_s	Scour depth [cm]
Q_{sed}	Total sediment load [g/min]
Q_{st}	Sediment loads in the main channel [kg/s]
Q_{st}	Sediment loads in the tributary [kg/s]
h_d	Flow depth of the downstream [cm]
Re_*	Boundary Reynolds number
τ_*	Dimensionless shear stress
u_{cr}	Critical shear velocity [m/s]
d	Grain diameter [m]
ν	Kinematic viscosity [m^2/s]
τ	Bed shear stress [N/m^2]
γ_s	Specific weights of sediment [N/m^3]
γ	Specific weights of water [N/m^3]
g	Gravitational acceleration [m/s^2]
u_*	Shear velocity [m/s]
H	Flow depth [m]
S_0	Initial bed slope
g_b	Bed material weight per unit width per unit time [kg/s/m]

q_b	Bed material volume per unit width per unit time [$m^3/s/m$]
τ_c	Critical shear stress [N/m^2]
q	Water weight per unit width per unit time [kg/s/m]
V	Cross-sectional velocity [m/s]
G_{gr}	Dimensionless sediment transport
F_{gr}	Dimensionless mobility number
D_{gr}	Dimensionless grain diameter
Q	Discharge [l/s]
C_d	Flow coefficient
b	Width of the weir [m]
P	Height of the weir [m]
h	Flow depth over the weir [m]
d_{50}	Median diameter [m]
σ_g	Geometric standard deviation
Q_{sr}	Right tributary sediment load [kg/min]
Q_{sl}	Left tributary sediment load [kg/min]
Q_r	Discharge of right tributary[l/s]
Q_l	Discharge of left tributary[l/s]
Q_m	Discharge of main channel[l/s]
Fr	Downstream Froude number
Re	Downstream Reynolds number
D	Hydraulic radius [m]
S_w	Slope of water surface

Chapter 1

Introduction

River confluences are locations where two or more rivers with the same or different flow rates and sediment characteristics merge and continue to flow as a single stream. Confluences are common occurrences along natural rivers and artificial open channels [1].

River confluences have symmetrical (Y-shaped) or asymmetrical planforms dependent on the angle between the two upstream tributaries and their orientation in relation to the downstream channel.

An asymmetrical river junction occurs when a main channel flow combines with a tributary flow coming from another direction and continues its way by increasing its flow downstream of the confluence (see Figure 1.1).

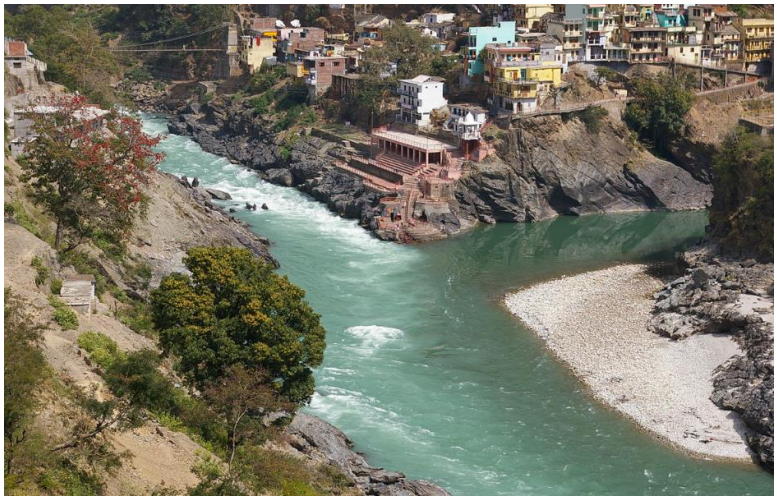

Figure 1.1: Asymmetrical river confluence [2]

The merging of the two tributaries to form the main channel is called symmetrical river confluence. The angles of deflection about a centerline projected upstream along the center of the downstream channel define the symmetry degree of confluence (see Figure 1.2).

Figure 1.2: Symmetrical river confluence [3]

At a confluence, hydrodynamics, sediment transport processes, and morphodynamics influence and modify each other. The flow structure in the confluence hydrodynamic zone interplays patterns of sediment transport, which results in the bed morphology changes [4]. Because of these changes, confluence poses risks associated with flooding, bank erosion, problems for navigation, and failure of the bridge or structures nearby [5]. Confluence morphodynamics may also affect critically channel and floodplain ecology [6]. Considering all these facts, the river confluences are of major importance within a range of disciplines.

For effective river management, river engineers, geologists, and city managers search better understanding of confluence-related problems. For this purpose, the hydrodynamic, morphological, and ecological structure at the river junctions has long been of great interest to fluvial scientists and hydraulic/river engineers. However, confluence hydraulics and associated bed morphology are complex as it is controlled by physical features including discharge ratio, junction angle, the presence

and nature of any bed discordance, the amount and of sediment load, and the gradation of sediment. [4, 7-9]. Some effects of these parameters on confluence hydraulics and associated bed morphology are explained below.

High discharge ratios, which means high flow rates in a tributary, cause migration of scour hole (see Figure 1.3).

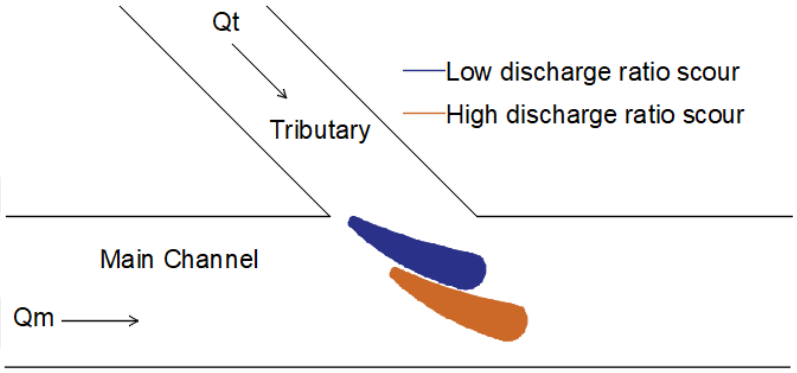

Figure 1.3: The effect of discharge ratios on scour holes

As in shown Figure 1.4, increase in junction angle, larger and wider bank-attached bar occurs.

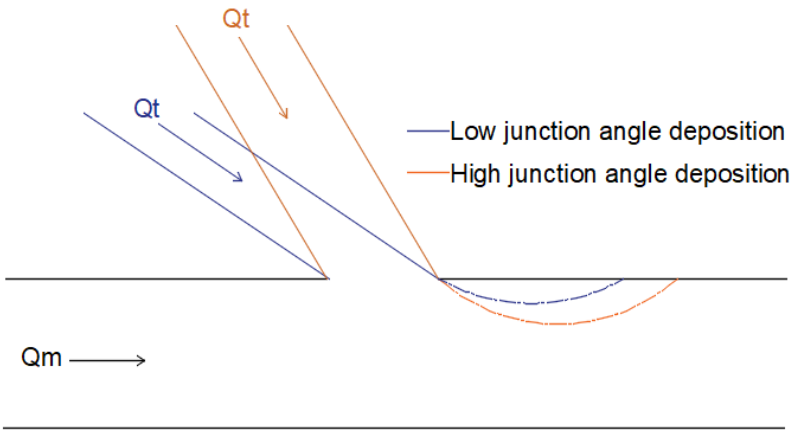

Figure 1.4: The effect of junction angles on bank-attached bars

A discordance in bed elevation between mainstream and tributary channels is a common feature of most river confluences. Biron et al. [9] carried out experiments in

the laboratory to identify the effect of bed discordance on flow characteristics. When a step is present, a very strong vertical motion exists immediately downstream from the tributary corner and contrasts markedly with the concordant bed case where all the vectors remain parallel to the bed (Figure 1.5).

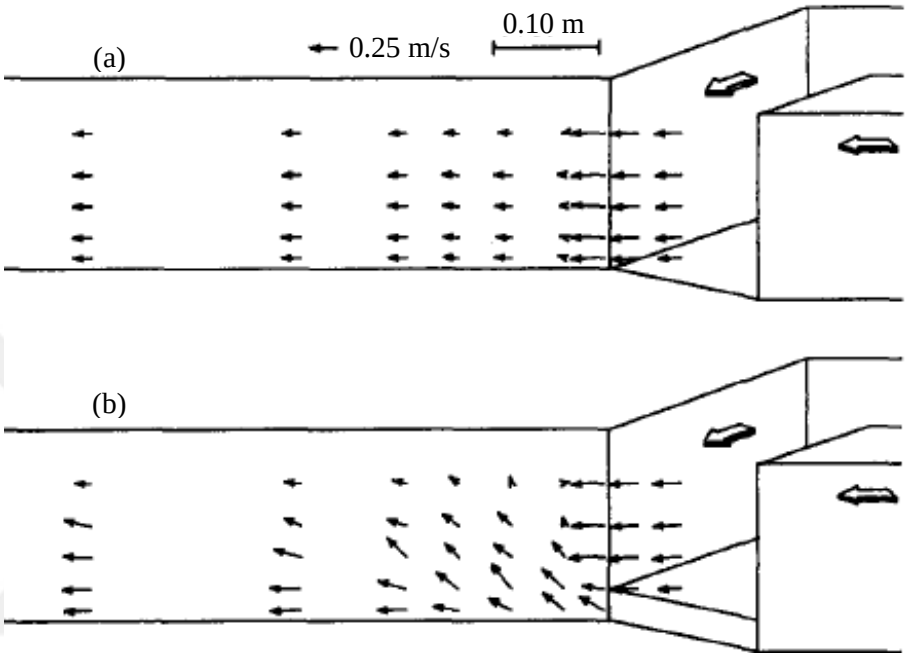

Figure 1.5: Plots of velocity vectors along a longitudinal section near tributary side wall, (a) Concordant Bed, (b) Discordant Bed [7]

Mosley [10] analyzed confluences with different sediment loads on an experimental set-up with dimensions 2.8 m long, 1.3 m wide and 0.12 m deep.The median diameter of sediment was 0.34 mm. The relation between maximum scour depth d_s (cm) and total sediment discharge through the confluence Q_{sed} (g/min) is shown in Figure 1.6. A set of six runs (series IIB) were done under different sediment loads in which confluence angle, tributary channel widths, and tributary discharges were held constant at 60°, 6 cm, and 125 cc/sec respectively, and in which total sediment loads were varied between 55 g/min and 220 g/min. Runs in series IIB were replicated twice. Series IIA runs with constant tributary discharges (125 cc/sec) and tributary channel width (6 cm) are also shown in Figure 1.6. There was a good relation between scour depth and total sediment load. It was observed that scour hole depth decreases as the total sediment load increases.

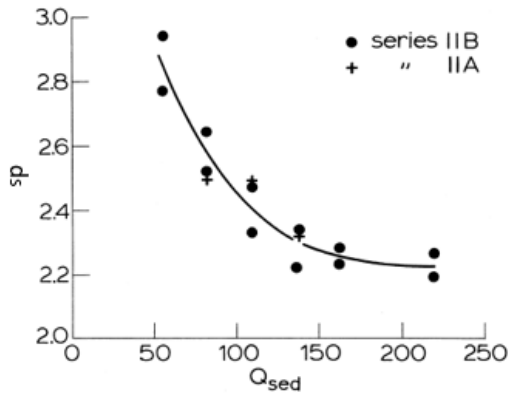

Figure 1.6: Relation between maximum scour depth and total sediment discharge [10]

Bombar and Cardoso [1] characterized the influence of sediment discharge on the morphology of movable bed, asymmetric, open-channel confluences. Fifteen experiments were performed by running a single combination of confluent discharges and using a single bed material, with three different sediment loads in the main channel (Q_{sm}) combined with five different sediment loads in the tributary (Q_{st}). According to the results of their experiments, the depth of the scour hole, d_s, decreased with $Q_{st.}$ The scour depth did not critically depend on Q_{sm} for Q_{sm} = [0.0033; 0.0100] kg/s although it was much smaller for Q_{sm} = 0 (see figure 1.7).

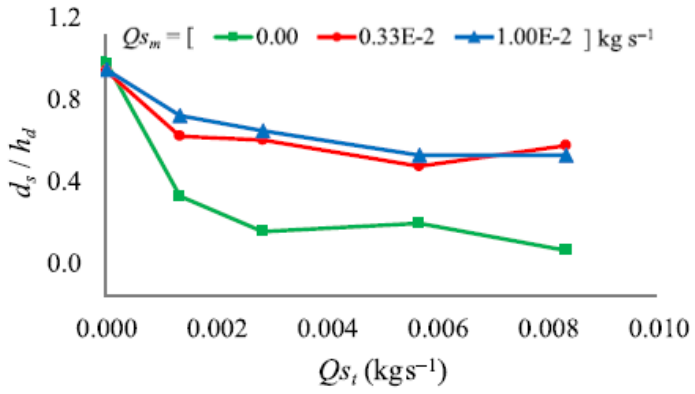

Figure 1.7:Variation of scour depth with sediment load in tributary and main channel [1]

The sediment gradation was another influential parameter on the hydro morphodynamics of the confluence. Guillén-Ludena [11] conducted experiments with uniform and non-uniform sediment feeding. The sediment rates were the same for all the experiments, 0.5 kg/min and 0.3 kg/min for the tributary and main channels, respectively. With non-uniform sediments (high gradation coefficient) the hydro-morphodynamics needed to evolve to convey the wide range of particle sizes of the sediment mixture. This evolution resulted in larger bank-attached bars, deeper scour holes, steeper tributary bed slopes, and steeper slopes of the water surface in comparison to the experiments performed with uniform sediments (low gradation coefficient).

When it is inspected carefully, it is observed that previous studies generally were carried out on small-scaled flumes like Mosley [10] who used cohesive sediments on a very small-scaled experimental set-up or which were conducted on asymmetrical confluences like Guillén-Ludena [11] and Bombar and Cardoso [1]. Only Guillén-Ludena [11] presented the time evolution of the bathymetry in the asymmetrical flume. But the variation of bed topography of a symmetrical confluence has not been studied which constitutes a necessity in understanding the effect of sediment transport on the time variation of the accumulations and the depositions. In order to close this gap, in this study it is aimed to identify the effects of sediment load on the time evolution of the morphology of a large-scale laboratory movable-bed symmetrical confluence when the flow is steady and non-uniform. The novelty of this thesis, would be the use of non-cohesive bed material on a relatively large experimental set-up and specifically investigation of a symmetrical movable bed confluence.

The present study consists of five chapters. Chapter 1 aims to present a brief introductory background to the research subject. The mechanism of sediment transport and formulations for bed load calculation and morphodynamics of confluences are summarized in Chapter 2. In Chapter 3, experimental studies are explained and summarized. The results of the experimental study and discussion are presented in Chapter 4. and the findings are declared in Chapter 5.

Chapter 2

Theory of Movable-bed Open Channels

2.1 Mechanism of Sediment Transport

Sediment deposition deals with water and sediment particles so, the physical properties of water (density, specific weight, viscosity) and sediment particles (size, shape, particle specific gravity, etc.) should be studied to understand the sediment transport mechanism.

When the flow conditions satisfy or exceed the criteria for incipient motion, sediment particles start to move and they are eroded from the basin by water and transported by stream.

To determine the critical point for the determination of the inception of motion of the grains Shields [12] derived a function where the balance of forces acting on a particle on a bed was considered. He applied dimensional analysis to determine dimensionless parameters and investigated the relationship between the boundary Reynolds number, Re_*, and dimensionless shear stress, τ_*, by experimental studies which are given in Equation (2.1) and Equation (2.2).

$$\mathrm{Re}_* = \frac{\mathrm{u_{cr}d}}{\nu} \tag{2.1}$$

$$\tau_* = \frac{\tau}{\gamma \Delta \mathrm{d}} = \frac{\mathrm{u_{cr}}^2}{\mathrm{g}\Delta \mathrm{d}} \tag{2.2}$$

Where, g is the gravitational acceleration, $\Delta = ((\gamma_s - \gamma)/\gamma$, and γ_s and γ are the specific weights of sediment and water respectively, d is grain diameter, ν is kinematic viscosity, u_{cr}.is the critical shear velocity.

Bed shear stress, τ, can be obtained from Equation (2.3).

$$\tau = \gamma H S_0 = \rho u_*^{\,2} \qquad (2.3)$$

The shear velocity, u_* , is expressed as in Equation (2.4).

$$u_* = \sqrt{gHS_0} \qquad (2.4)$$

Where, *H* denotes the flow depth, S_0 is the initial bed slope.

Vanoni [13] developed a diagram fitting the curve to the data provided by Shields (see Figure 2.1).

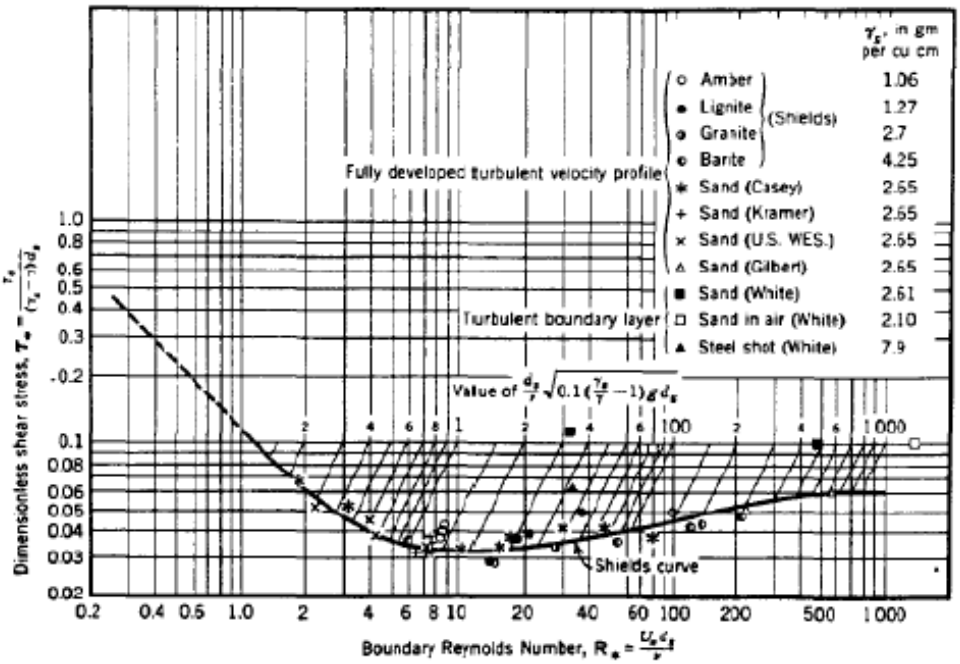

Figure 2.1: Shields graph [12]

The area below the curve in Figure 2.1 means that there is no sediment motion, whereas the area above the curve means that there is sediment motion. The curve gives the critical value of Shields parameter, τ_*, corresponding to the beginning of the motion.

By the help of the parameter defined in Equation (2.5), the usage of Shields curve becomes easier [11].

$$p = \frac{d}{\nu}\sqrt{0.1\Delta g d} \qquad (2.5)$$

This parameter allows the determination of intersection with the Shields diagram and its corresponding values of shear stress. Many investigators have proposed different options which are more or less the same.

Sediments are transported as suspended and bed load as shown in Figure 2.2 depending upon the fundamental properties of water and sediment particles.

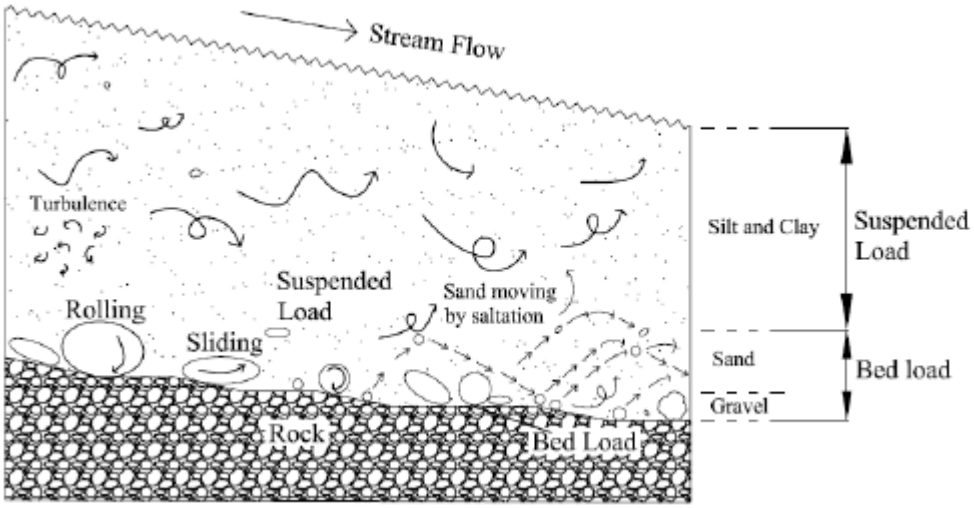

Figure 2.2: Different modes of sediment transport [14]

In a river system, a loose surface can erode from the basin by water and be transported by stream. Sediment particles can be transported in four modes rolling, sliding, saltation and suspension. While sediment particles are sliding and rolling, particles continue to be at contact with the bed. Saltation means that jumping motion

along the bed in a series of low trajectories. Rolling and sliding particles move along the bed surface under the force of the overlying flow of water. These three modes are bed load transport. Sometimes sediments stay in suspension for an appreciable length of time called suspended load transport. In addition, the wash load is a bed material load according to the particle size and mainly moves as a suspended load. So, sediment can be classified as bed material load and wash load or bed load and suspended load. Wash load transport is a function of basin characteristics, whereas bed load transport is a function of flow characteristics [15].

Bed load motion starts when critical conditions are exceeded. The motion concerned with two phase (solid + liquid) flow near the bed. Generally, the bed load transport rate of a river is about 5-25% of that in suspension. Bed load measurement is difficult, so it is estimated by sediment transport formulas based on different modes of motion employing different parameters.

Bed load transport is defined as the bed material weight per unit width per unit time, g_b (kg/s/m) or the volume of the transported bed material per unit width per unit time, q_b (m^3/s/m) where the relationship between them is given in Equation (2.6).

$$g_b = \gamma_s q_b \tag{2.6}$$

Up to now, several empirical formulas of transported bed load have been developed. Most of these formulas estimating bed load, have been proposed for uniform flow and uniform bed conditions. The empirical formulas derived for bed load calculation are given below.

Duboys [16] developed a bed load model using the shear stress approach. This model consists of sediment particles moving in layers because of the tractive force acting along at the bed. The bed load capacity formula is given as Equation (2.7).

$$q_b = K\tau(\tau - \tau_c) \tag{2.7}$$

Where, Straub [17] defined *K* coefficient as in Equation (2.8) depending on the sediment particle characteristics, τ_c is critical shear stress.

$$K = \frac{0.173}{d^{3/4}} \tag{2.8}$$

Thus, DuBoys equation can be rewritten as in Equation (2.9),

$$q_b = \frac{0.173}{d^{3/4}} \tau(\tau - \tau_c) \tag{2.9}$$

Meyer-Peter et al. [18] developed the following bed load formula as given Equation (2.10) uses the energy slope approach.

$$\frac{0.4 q_b^{2/3}}{d} = \frac{q^{2/3} S_0}{d} - 17 \tag{2.10}$$

where, *q* denotes the water weight per unit width per unit time (kg/s/m).

Meyer-Peter formula is valid only for coarse material sediment particle diameters greater then 3 mm.

Shields [12] conducted laboratory studies and obtained the flow conditions corresponding to incipient motion when sediment transport is greater than zero. Shield's measurements provided a semi-empirical equation, as given in Equation (2.11), for estimating bed load transport capacity.

$$\frac{q_b \gamma_s}{q \gamma S_0} = 10 \frac{\tau - \tau_c}{(\gamma_s - \gamma) d} \tag{2.11}$$

Ackers and White [19] proposed a procedure that can be used for the estimation of total bed material load in both natural rivers and laboratory channels. Transported sediment mass per unit flow mass, X, is calculated as in Equation (2.12),

$$X = G_{gr} \frac{d}{h_d} \frac{\gamma_s}{\gamma} \left(\frac{u_*}{V}\right)^{2/3} \tag{2.12}$$

where, *V* denotes the cross-sectional velocity (m/s).

Dimensionless sediment transport, G_{gr} , is expressed as in Equation (2.13).

$$G_{gr} = C\left(\frac{F_{gr}}{A} - 1\right)^{m} \qquad (2.13)$$

Dimensionless mobility number, F_{gr} , is expressed as in Equation (2.14).

$$F_{gr} = {u_*}^{n}(gd\Delta)^{-1/2}\left(\frac{V}{\sqrt{32}\log\left(\frac{10h_d}{d}\right)}\right)^{1-n} \qquad (2.14)$$

where, *C*, *A*, *m* and *n* are constants and can be calculated by the dimensionless grain diameter, D_{gr}, given in Equation (2.15)

$$D_{gr} = d(g\Delta/\nu^2)^{1/3} \qquad (2.15)$$

The values *C*, *A*, *m* and *n* can be obtained from laboratory data in Equation (2.16).

$$D_{gr} > 60 \quad \begin{matrix} m=1.5, \\ n=0 \\ A=0.17, \\ C=0.025 \end{matrix} \qquad (2.16.a)$$

$$1 < D_{gr} \leq 60 \quad \begin{matrix} n=1-0.56\log(D_{gr}) \\ m=(9.66/D_{gr})+1.34 \\ A=\left(\frac{0.23}{\sqrt{D_{gr}}}\right)+0.14 \\ \log C=2.86\log(D_{gr})-(\log D_{gr})^2-3.53 \end{matrix} \qquad (2.16.b)$$

2.2 Morphodynamics of Confluences

The sediment load in the tributaries is also an important factor on bed morphology of the confluence. Deposition in the backwater zone adjacent to the area upstream of the confluence increases depending on the increase in the sediment load.

In the existent first studies on river junctions, Taylor [20] studied the confluence hydrodynamics. He worked on the flow characteristics of rectangular channels. The experiments were performed with 45˚ and 135˚ junction angles. The purpose of the experiments was to estimate the relationship between upstream and downstream flow

depths and energy head-losses in the confluence. In this study, one-dimensional modeling was obtained which was based on mass and momentum conservation and wall-friction roughness was neglected. The results of the experiments showed that the difference between the flow depths obtained by using the momentum equation and the result of the experiments decreases when the junction angle decreases. Also, Webber and Greated [21] worked on hydrodynamics using one-dimensional approach. Empirical correction coefficients are needed in these models, due to the real flow characteristic of river confluence is three-dimensional.

With the development of measuring instruments and computer technologies over time, three-dimensional flow structure, sediment transport, and riverbed evolution, located in the river confluence, have been captured and described accurately [22]. After the 1980s, more and more studies have been done on the hydrodynamic, morphologic, and morphodynamic structure at river junctions, including laboratory experiments, field experiments, and numerical simulations.

Based on flow visualization in small-scale models, the cross-stream flow structure was researched for simple Y-shaped confluences in a laboratory channel by Mosley [10]. In this experimental work, the flume used in the study was 2.8 m long, 1.3 m wide, and 0.12 m deep. In order to define flow patterns, the dye was injected into the tributaries. Dye injection showed that the flows from the tributaries generally separate through the scour with some mixing along the center. Although the flowlines were parallel to the banks in tributaries, a flow deflection was observed within the limits of the scour hole in the confluence.

Best [8] carried out laboratory experiments in order to determine the flow structure of asymmetrical confluences. Experiments were conducted in a facility with an 8 cm wide tributary connected at a 30˚ junction angle to a 12 cm wide main channel with a fixed and flat bed and proposed a conceptual hydrodynamic model according to the results of experiments which was characterized by the presence of zones of stagnation, deflection, separation, maximum velocity, recovery, and two shear layers.

Ashmore et al. [23] made velocity measurements in two confluences in the gravelly Sunwapta River. In both cases, confluences have simple Y-shaped planforms which were obviously formed and still active. Although a separation zone is observed

downstream of the confluence corners in laboratory channels with rigid boundaries, there was an obvious separation zone only on the left side at one of the confluences [10]. Because of the more gentle curvature of the corners of natural confluences limited the formation of the separation zone [24]. Flow diverged and divided again a short distance downstream of both confluences. Also, some evidence of flow acceleration into the confluence was obtained.

Based mainly on experimental work, general conceptual models of confluence hydrodynamics have been developed for symmetrical and asymmetrical confluences [8,10] (see Figure 2.3).

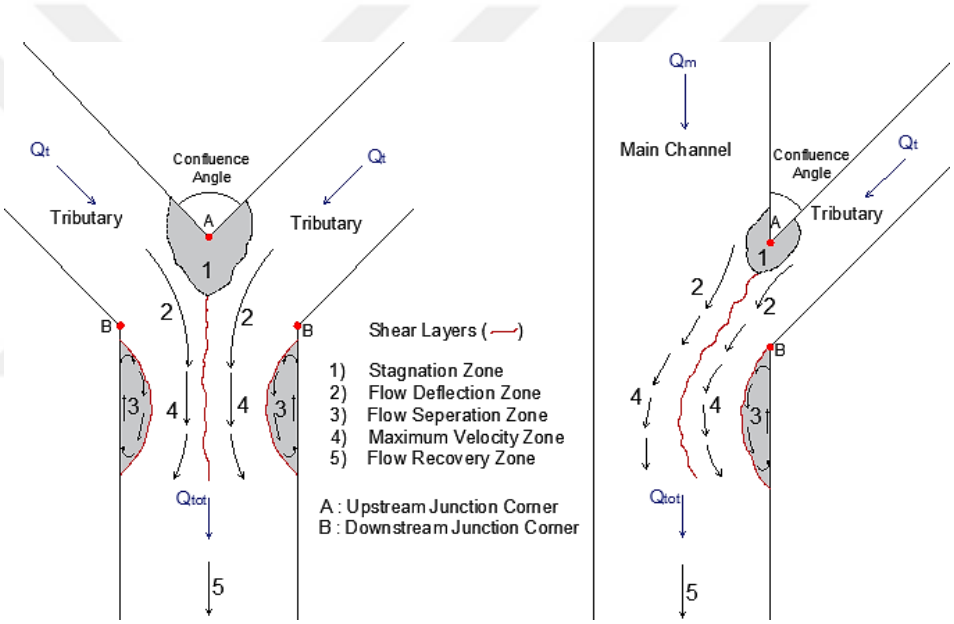

Figure 2.3: Hydrodynamics at open-channel confluences, (a) Symmetrical, (b) Asymmetrical

The hydrodynamics at the confluence is different from that of ambient flows because two merging flows have different flow characteristics.

As shown in Figure 1.5, a **zone of flow stagnation**, or at least deceleration of flow, occurs at the upstream corner of the confluence because the flow depth increases where the combining flows meet [25]. As flow encounters the adverse pressure gradient related to this super-elevation of the water surface, forward motion is

inhibited and the flow decelerates. The flow velocity and shear stress decrease and flow depth and pressure increase in this region.

Within the confluence, a **flow deflection zone** is formed due to combined flows mutually deviate one another. If the amount of suspended material transported by the combined flows is different, a visible mixing layer begins to form along an interface [26]. The mixing layer continues along the separation zone. This mixing interface is also the location where the **shear layer** is formed when the confluent flows have dissimilar velocities. This layer is known for high turbulence intensity and shear stress.

A **zone of flow separation** takes place at the downstream junction corner originated by the change of flow direction. This change results from the main flow being pushed towards the outer bank by the lateral flow. This separation zone extends over a distance in the downstream channel [27]. Although the separation zone is commonly observed in laboratory applications with sharp angles, rounding or flaring of junction corners (a common feature of many natural confluences) prevents separation [28]. This region is characterized by flow recirculation and low pressures. The zone is known to increase in size with larger junction angle and high tributary discharges [29].

It is observed that the vertical velocities become significantly more pronounced in the upward direction. These vertical velocities act as a water barrier (a **shear layer** occurs between the recirculation zone and surrounding main channel flow) and prevent entering the main channel flow from this shear layer. Thus, downstream of the mixing point, the cross-section of the water flows becomes narrower, the effective width decreases, resulting in greater velocities (maximum velocity). As the cross-sectional area of the flow decreases, the cross-sectional average velocity increases even more, and **maximum velocity zone** is located in this region [30].

As the flow moves downstream, the influences of confluence hydrodynamics reduce and a **flow recovery zone** occurs where the hydraulic conditions become governed by receiving channel characteristics.

Biron et al. [31] investigated patterns of micro-topography of the water surface at symmetrical and asymmetrical discordant confluences in the field for different flow

conditions. According to the results of this study, a super-elevation was observed in the flow stagnation zone and in the mixing layer. Also, there is a lateral slope at the edge of the mixing layer.

The first study of river confluence morphology was performed by Mosley [10] both in symmetrical and asymmetrical confluences in a small flume under movable bed conditions. The experiments were carried out with different discharge ratios, junction angles, and amounts of sediment feeding. Based on these experiments, although the dunes fronts in both tributaries were perpendicular to the flow direction, they rotated parallel to the flow in the main channel, around the scour hole. It was observed that the presence of scour a hole in the confluence of both symmetrical and asymmetrical confluences. The transported sediment formed a sediment deposition zone downstream of the confluence. Also, according to these experiments, it was observed that scour hole depth decreases as the total sediment load increases. In addition, when the difference between the two tributaries' discharges decreases, the depth of scour increases and it reaches maximum value while discharges are equal. Depth also rises with increasing confluence angle.

The experimental and field measurements done by Ashmore and Parker [7] for a braided river show that the confluence angle has the most effect on scour hole dimensions. An increase in total discharge, confluence angle (between 30 degrees and 90 degrees) or grain size can increase scour depth.

Best [32] investigated sediment transport at the asymmetrical confluence both in scaled laboratory flume and in nature. 5 different junction angles (15˚, 45˚, 70˚, 90˚ and 105˚) were chosen both to simulate the most common ones in natural environment as determined from map analyses [33] and to cover a wide range. The experiments were conducted under movable bed conditions at 3 different discharge ratios (approximately 0.5, 1.0 and 1.5). Sediment was continuously supplied to both channels during the experiments. Each experiment was continued until the equilibrium conditions were reached. Field studies were carried out confluence of River Ure and Widdale Beck in North Yorkshire, UK.

Based on the experiments of Best [32], the bed morphology at the confluence consists of 3 distinct elements: avalanche faces at the mouth of each confluent

channel, a region of central bed scour at the confluence, and a bar formed in the separation zone located at the downstream corner of the confluence. Field measurements closely replicate the flume simulation. In addition, it is observed that when both the junction angle and discharge ratio increase, the penetration of the main channel avalanche face decreases. As the joining angle rises, a deeper scour hole was formed, there was no scour hole formed in the experiment performed at a 15˚ angle, and the rate of increase in scour depth declines at higher angles. Deeper scours were present at higher discharge ratios for all confluence angles. As the confluence angle and discharge ratio increase, the bank-attached bar became larger related to the formation of a larger separation zone.

Best and Rhoads [34] identified a conceptual model to describe the bed morphology of river confluences by using most of the existent knowledge on the confluence morphodynamics provided by field junctions at different scales and experimental works performed within fixed-wall channels and also within completely movable beds. Five principal morphological features can be defined at channel confluences, despite these features presence/absence being dependent on a range of control parameters: a scour hole, tributary mouth bars, a mid-channel bar, a bank-attached bar, and a sediment accumulation zone.

Based mainly on experimental work, general conceptual models of confluence morphology have been developed for symmetrical and asymmetrical confluences (see Figure 2.4).

There is a close interaction between hydrodynamics, morphodynamics, and sediment transport at the river confluence. So, the structure of flow at confluences produces patterns of scouring and accumulation, in turn, shape the bed morphology of the confluence [35].

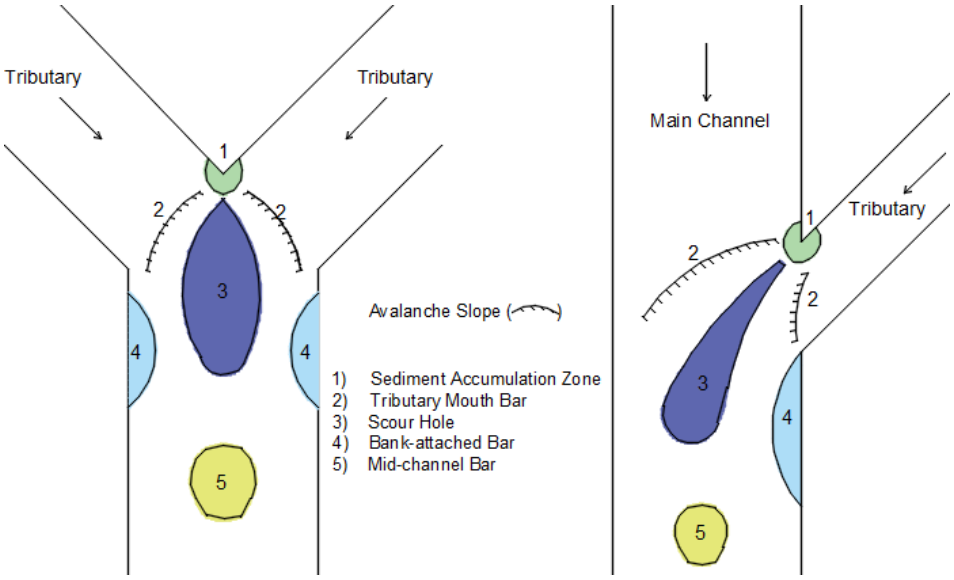

Figure 2.4: Bed morphology at open-channel confluences, (a) Symmetrical, (b) Asymmetrical

A local **sediment accumulation zone** occurs depending on the obstruction of sediment transport because of the flow stagnation at the upstream junction corner. Considering low velocities, bed surface sediment is finer than adjacent channels. No significant bar forms occur in this region.

Sediment accumulated at the mouth of one, or both confluent channels, widely is referred to as **tributary-mouth bars**. Sometimes, the fronts of these bars merge with the side slopes of the scour hole and may migrate into the scour hole, filling it partially. If the bar front slope is quite steep, approaching angle of repose of bed material, resulting in **avalanche surfaces**.

Confluence scour takes place commonly in braided sand-bed or gravel-bed rivers, but can occur wherever two branches of a river merge and create secondary erosive flows [36, 37]. There are several factors affecting scour at confluences, including convective acceleration of flow, and increased turbulence along the shear layer. With the accelerating of effective flow from upstream to downstream through a confluence, bed shear stress and sediment transport capacity increase over distance, resulting in the scouring of bed material. Although in symmetrical confluences, the scour hole is symmetrical in planform shape, it extends from the tributary mouth to the outer bank of the post-confluence channel in asymmetrical confluence.

Biron et al. [38] reported that the scour may be small or absent in confluence where there is a discordance in bed height between two tributaries. Depths of scour in large rivers are generally smaller than in small streams and experimental channels for a given junction angle [34]. Nevertheless, scour depths at the confluence in large rivers can reach 70 meters [39].

Experimental studies indicate that as the width ratio increases, scour depth decreases [40].

A **bank-attached bar** may form in the region of flow separation dependent on recirculation or reduced flow velocities [41].

Zhang et al. [42] investigated bed morphology at a naturally asymmetrical confluence of a tributary with a low sediment load and the main river with a high sediment load and very large momentum flux differences with a discordant bed. The confluence of the Yellow River and Fen River was selected for field measurements. According to obtained data, no significant sand bar was observed because of the lack of flow separation.

A deposition is often observed in the middle of the post-confluence channel, mostly in symmetric confluences (Y shape planform) that is called **mid-channel bar**. If a scour forms in the upstream region, the decreasing flow velocities downstream from the maximum velocity zone, as well as reducing turbulence intensities as the shear layer disappears [43] will unavoidably lead to sediment accumulation.

Guillén-Ludena [11] investigated the effects of channel width ratio on morphodynamics at rivel confluences in the laboratory. The experiments were conducted in the main flume which was 12 m in length, 1 m, and 0.5 m in width (two conditions) and the tributary was 4.5 m in length, 0.15 m in width. The junction angle between the main channel and tributary was 70˚. The experiments were done under movable bed condition and sediment were continuously fed to both channels during the experiments. The downstream flow depth was adjusted to 10 cm. For this study, 6 experiments were carried out with 3 different flow rates and 2 different width ratios. It was observed that increasing discharge ratios resulted in longer, wider and higher bank-attached bars and deeper scour holes at the tributary mouth in when the main channel has a 0.5 m width. As increase width of the main channel, a larger

bank-attached bar occurs due to a more developed zone of separation at the downstream junction corner.

Shakibaeinia et al. [44] and Shakibaeinia et al. [45] used a 3-D numerical model to reflect the sediment transport and bed morphology in the laboratory-sized and field confluences in a wide range of confluence angles and discharge ratios. They obtained that with a decrease in confluence angle as well as an increase in discharge ratio, the size of scour hole can reduce, and its location move to further downstream in the main channel.

Yu et al. [46] performed laboratory experiments in a novel confluence flume under movable bed conditions until the initial equilibrium of bed geometry and then fixed. After that point, colored sediment of fine gradation which reflects the contaminated sediment was fed into the tributary channel. This study described the morphodynamics and deposition patterns of contaminated sediments in a confluence as a function of junction angle and discharge ratio. The results showed that the junction angle was a dominant factor that defined the confluence bed morphology and sediment transport while the discharge ratio was a secondary factor. If the fed sediment amount were relatively small, under different junction angles and discharge ratio conditions, the whole sedimentation pattern was similar to the corresponding equilibrium bed morphology pattern of confluences. According to the results, the contaminated sediments coming from a tributary tended to deposit and accumulate in the depositional areas within the junction. Also, it is observed that a corner scour hole is probably due to spiral vortices near the downstream junction corner all of the junction angle and discharge ratio confirmations.

Balouchi et al. [47] investigated the effects of bed load amount on the morphodynamic of channel confluence. The experiments were carried out a main channel with a length of 9 m, a width of 0.25 m and a tributary channel with the length of 3 m, the width of 0.25 m. Two experiments were conducted with the same hydraulic conditions, but different amount of bed load under live bed conditions. They obtained the 2D topography contour maps that no point bar or deposition of sediments occur at the confluence. Bed morphologies were different with and without bed load. It is observed that a deeper scour hole was formed with no sediment feeding.

Chapter 3

Experimental Set-up, Instrumentation and Procedure

In this chapter, the experimental set-up, the measuring instrumentation and equipment, the bed material characteristics, the experimental procedure, and the measurements adopted for the present research study are described.

3.1 Experimental Set-up

Experiments are carried out in Izmir Kâtip Çelebi University, Civil Engineering Hydraulics Laboratory (see Figure 3.1).

Figure 3.1: General view of the experimental set-up

The experimental setup is a symmetrical confluence which consists of a main channel with a length of 18 m, a width of 2 m, and a depth of 0.88 m; and two

tributaries, both of which have the same characteristics, with a length of 4.92 m, the width of 1 m and the depth of 0.88 m (see Figure 3.2).

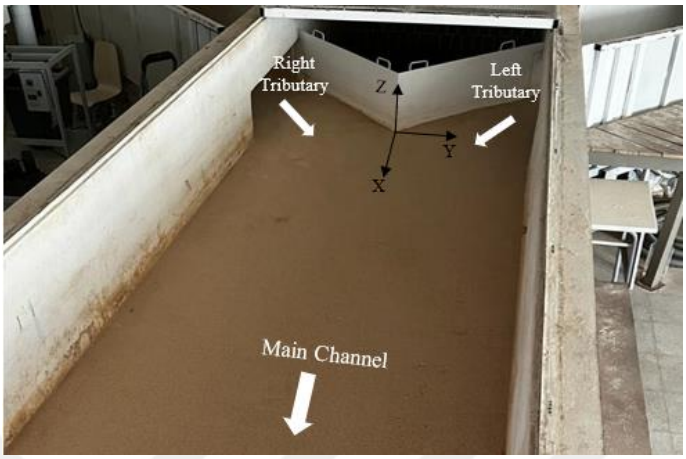

Figure 3.2: Experimental facility at the laboratory

The junction angle between the main channel and the tributaries is 90°. The main channel and tributaries have rectangular cross-sections, reinforced concrete walls, and horizontal beds. 20 cm brick walls are built at x = 6.5 m, x=8 m and x=11 m in order to form the movable bed condition. The plan view of the set-up is given in Figure 3.3.

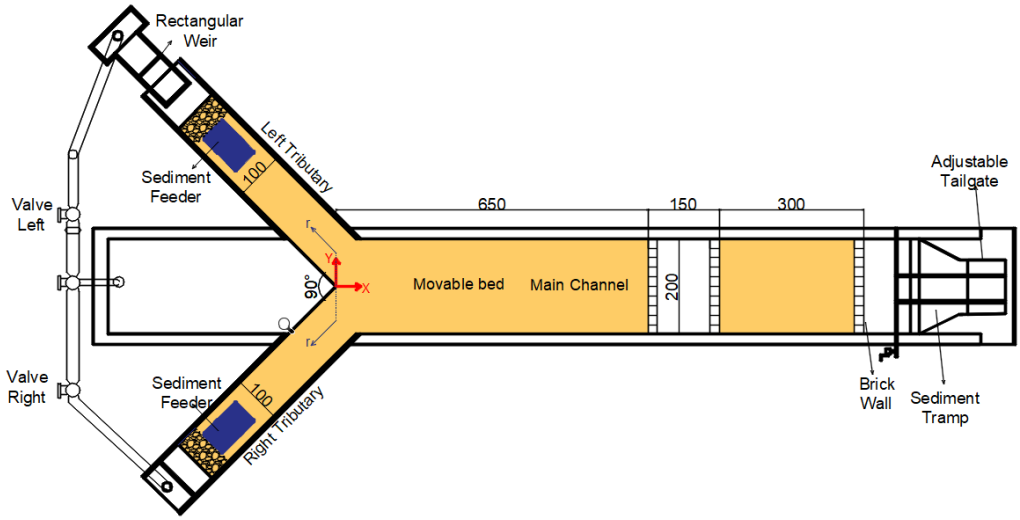

Figure 3.3: Plan view of experimental set-up (all units are cm)

The cross sections of the tributaries and the main channel are shown in Figure 3.4.

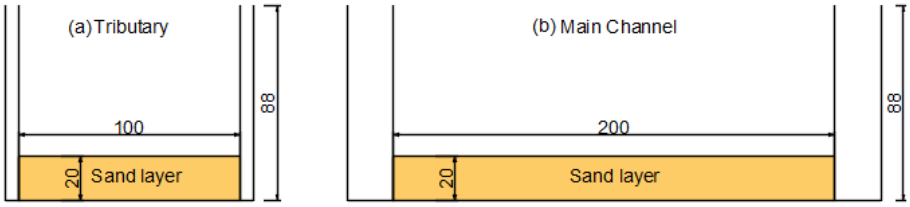

Figure 3.4: Cross sections (a) Tributaries, (b) Main channel

There is a water reservoir with 24 m^3 capacity and 2 centrifugal pumps with 15 kW power in the basement of the laboratory. The water is pumped out from the water reservoir and circulates in the experimental set-up with help of two pumps. One of these pumps supplies water to the right side tributary and the other pump supplies water to the left tributary (see Figure 3.5)

Figure 3.5: Centrifugal pumps for water supply to (a) Right tributary, (b) Left tributary

The water supplied to the system flows along the channel and reaches the circulation reservoir through the iron pipes from the downstream of the main channel and then

returns to the water reservoir from the circulation tank. It circulates continuously along the line (see Figure 3.6).

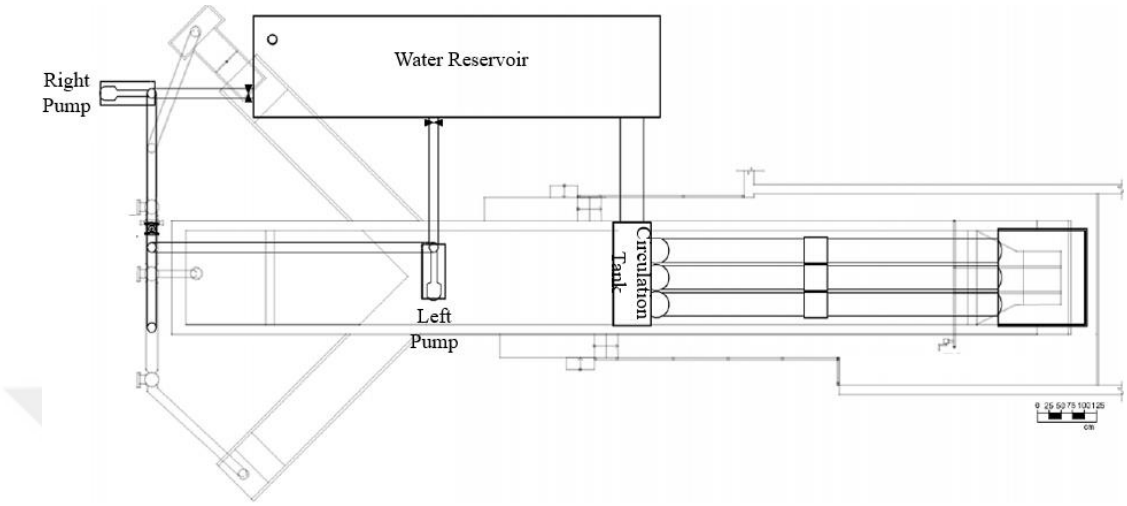

Figure 3.6: The plan view of the basement of the laboratory

The circulation tank is a part of the system between the channel and the water reservoir that stores the water coming from downstream of the main channel (see Figure 3.7).

Figure 3.7: The basement view of the laboratory

A unit controls the pump rotation speed in order to regulate the discharge of flow for the right tributary. Also, the flow rate in the pipe can be adjusted by using a valve and it is measured during the experiment by using an electromagnetic flowmeter (ORTİFLUX 1000 by Krohne) which is installed on the inlet pipe in which the water flows from the storage tank to right tributary via the centrifugal pump (see Figure 3.8). It can measure the flow rate with 0.1 l/s precision.

Figure 3.8: Control board for right tributary

The other pump works by turning the manual button on the board. The flow rate in the pipe can be adjusted by using a valve for the left tributary and there is a rectangular weir at the tributary inlet to control the supplied flow discharge (see Figure 3.9).

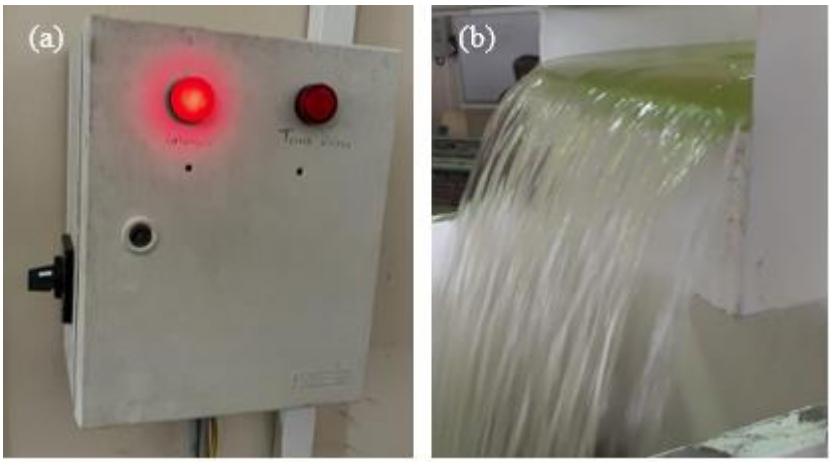

Figure 3.9: (a) Control board for left tributary, (b) Rectangular weir

Flow is measured with a limnimeter on the rectangular weir. The water depth over the weir is calculated using the Rehbock equation for rectangular weirs given in Equation (3.1) and Equation (3.2) (see Figure 3.10).

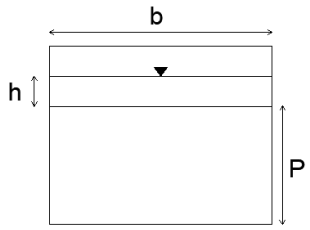

Figure 3.10: Front view of the rectangular weir

$$Q = C_d \frac{2}{3} \sqrt{2g} b h^{3/2} \quad (3.1)$$

$$C_d = 0.602 + 0.83h/P \quad (3.2)$$

where, Q denotes the discharge of flow, C_d is the coefficient of flow, g is the gravitational acceleration, b is the width of the weir, P is the height of weir (29.6 cm) and h is the depth of the flow over the weir (6.37 cm).

The flow depth throughout the flume can be adjusted by the tailgate at the downstream end of the main channel. It is controlled with a limnimeter to keep it constant during the experiments (see Figure 3.11).

Figure 3.11: (a) Adjustable tailgate, (b) Limnimeter

Two conveyor belts are used to supply sediments to the upstream of both tributaries. The conveyor belts have the same physical features which are 1 m in length and 0.6 m in wide (see Figure 3.12). It will be ensured that the added sand is equal across the cross-section of the tributaries.

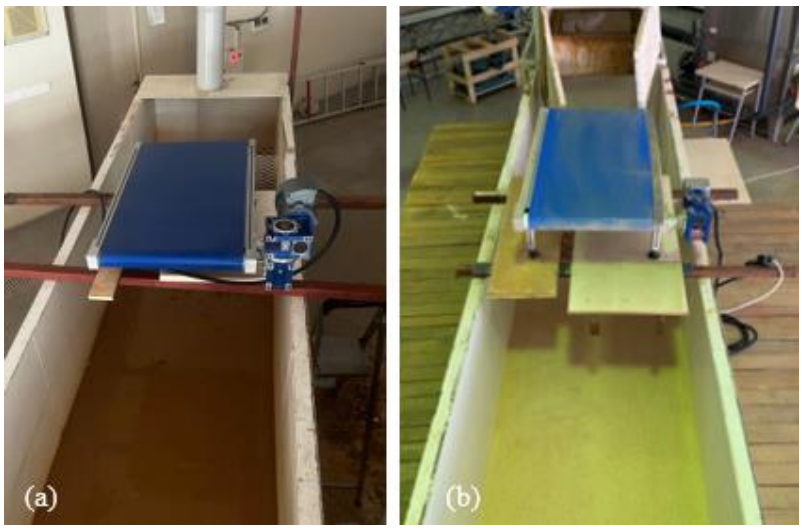

Figure 3.12: Conveyor belts (a) Right, (b) Left

3.2 Instruments and Equipments

3.2.1 Flowmeter

The supplied flow discharge of one of the tributaries (right) is measured by an electromagnetic flowmeter which is mounted on the pipe. The measured discharge has ± 0.1 l/s accuracies (Figure 3.13).

Figure 3.13: (a) and (b) Electromagnetic flowmeter

3.2.2 Acoustic Doppler Velocimeter (Vectrino)

Vectrino uses the Doppler Effect to measure flow velocity in water. The purpose of it in this study is to obtain the bottom scour depths (Figure 3.14).

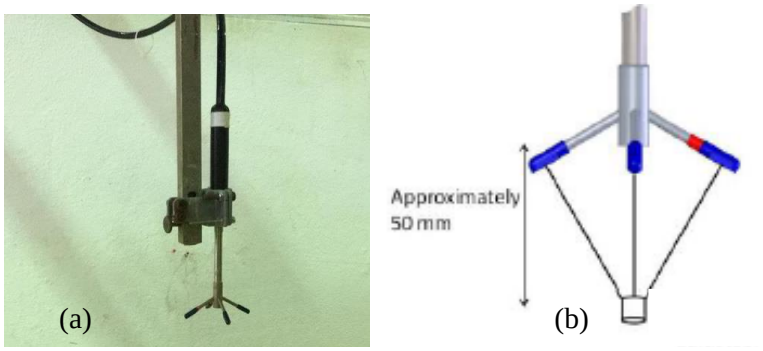

Figure 3.14: (a) and (b) Down-looking Vectrino

A down-looking acoustic doppler velocimeter (Vectrino) is used to measure bed topography. It has a three-dimensional sensor with remote sensing. Combined with Vectrino Plus software, it has a sampling rate of 200 Hz. The diameter of the received sound sampling is 6 mm. The Vectrino can receive data at a distance of 50 mm from the probe. Down-looking Vectrino uses four receivers (one in the x direction, one in the y direction, and two in the z direction) whereas side-looking uses three receivers. Vectrino obtains three-dimensional speed data with the data collected in the receivers. The probe of Vectrino works in water and provides a continuous flow measurement, focusing on a common sample volume. The system operates by transmitting short acoustic pulses along the transmission beam. As the pulses move along the water column, some of the acoustic energy is scattered back by small particles suspended in water. The measured distance has ± 0.1 cm accuracy.

3.2.3 UltraLab ULS-40D

UltraLab ULS-40D is designed for the measuring of water surfaces in Ship Model Basins, Flumes, Hydraulic Laboratories at Universities and Institutes and Simulation Facilities of Physical Models. It is an easy-to-handle airborn ultrasonic measuring system, which measures water level and waves fast and precisely (Figure 3.15). The ULS 40D system is equipped with fully assembled independent channels.

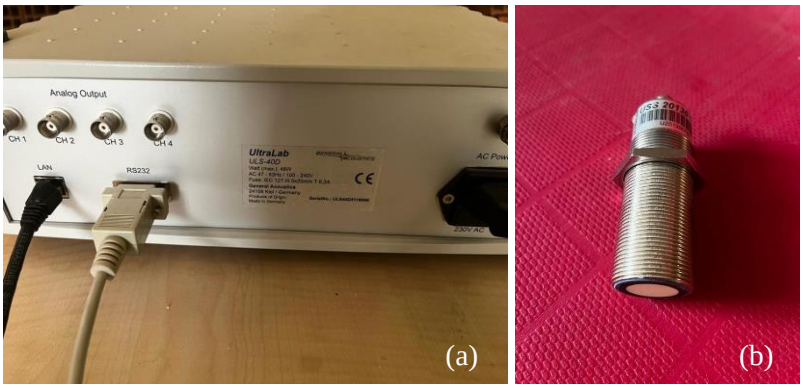

Figure 3.15: ULS-40D equipment (a) ULS-40D and (b) probe

UltraLab ULS-40D probes are used to measure the water surface with ± 0.1 mm accuracy (Figure 3.16).

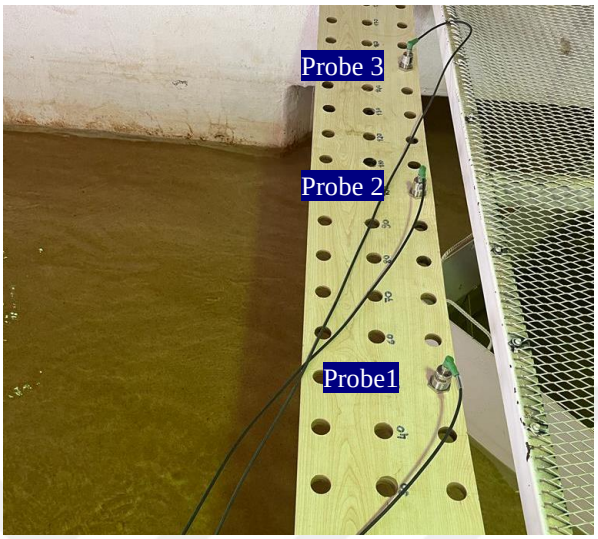

Figure 3.16: ULS-40D probes while measuring

3.2.4 Digital Scale

The amount of feeding sediment is adjusted with a digital scale (Figure 3.17).

Figure 3.17: Digital scale

3.2.5 GoPro Camera

At the end of the experiments, photographs are taken using a GoPro camera which shows the plan view bathymetry along the main channel (Figure 3.18).

Figure 3.18: GoPro camera

3.3 Bed Material Characteristics

The sediment used in this research study is uniform graded material which is characterized by the median diameter (d_{50}) and the geometric standard deviation of the material (σ_g). The value of d_{50} is 1.044 mm and σ_g is 1.16.

The grain size distribution of the bed material and supplied sediment mixtures is obtained as Figure 3.19.

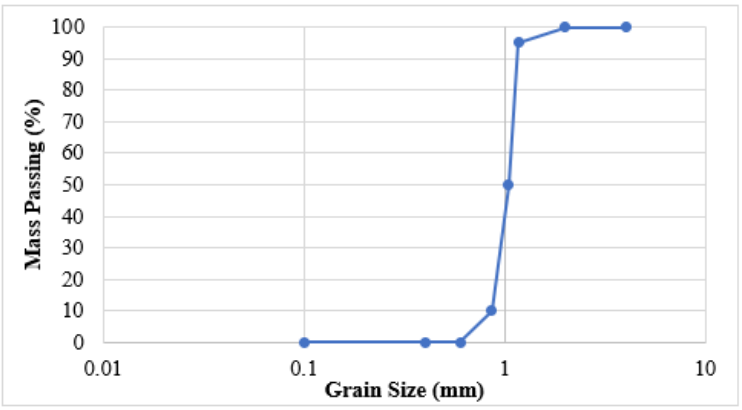

Figure 3.19. Grain size distribution of sediment

According to the results of [12] and [13] formulas, u_{cr} are calculated as 0.036 m/s.

3.4 Experimental Procedure

In this thesis, two experiments with the same hydraulic conditions, but 2 different sediment feeding rates (the right tributary, $Q_{sr,}$ and the left tributary, Q_{sl}) from tributaries in a symmetrical channel confluence.

The parameters kept constant within the scope of this study are the junction angle between the tributaries of the symmetrical river confluence, width of the tributaries and the main channel, flow depth downstream of the main channel, sediment type which is uniform and discharges in the tributaries and the main channel (the right tributary, Q_r, the left tributary, Q_l and the main channel, Q_m). The characteristic variables of this experimental study are summarized in Table 3.1. Also, downstream Froude number (Fr) and Reynolds number (Re) are given in Table 3.1.

Downstream Froude number (Fr) and Reynolds number (Re) are calculated as Equation (3.3) and Equation (3.4), respectively.

$$Fr = \frac{V}{\sqrt{gh_d}} \tag{3.3}$$

$$Re = \frac{VD}{\nu} \tag{3.4}$$

Where, D is hydraulic radius.

Table 3.1: Summary of the context of the experimental study

Q_r (l/s)	Q_l (l/s)	Q_m (l/s)	No	Q_{sr} (kg/min)	Q_{sl} (kg/min)	V (m/s)	Fr	Re (10^6)
20	20	40	E1	0	0	0.4	0.57	4.6
			E2	0.1	0.1	0.4	0.57	4.6

The flow depth downstream of the main channel was 5 cm for both experiments.

Both experiments were carried out following the same procedure. Before each experiment, in order to achieve the main goals of this study, the colored area shown in Figure 3.3 (main channel and tributaries), was covered with uniform sediment

which is 20 cm depth to ensure the movable bed condition. The surface of the sediment is leveled by an apparatus, which can move along the main channel (see Figure 3.20).

Figure 3.20: The apparatus to obtain a horizontal bed along the main channel

The 1.5 kg of sand was distributed on the left conveyor belt every 15 minutes. The 6.5 kg of sand was distributed on the right conveyor belt every 65 minutes ($Q_{sr}=Q_{sl}=0.1$ kg/min) (see Figure 3.21).

Figure 3.21: Distributed sediment for feeding (a) Left, (b) Right

At the beginning of each experiment, the tailgate downstream of the main channel was closed and the pumps started. The flows entered the tributaries slowly in order to avoid the initial movement of sediment (see Figure 3.22).

Figure 3.22: Filling of channel slowly

During the filling of the flumes, the tailgate was kept closed. When the flow depth reached to a certain height that will not move the sediment, the flow rates gradually increased for both tributaries up to the required discharge (20 l/s) of flow by using the valves (see Figure 3.23).

Figure 3.23: Filled channel downstream

After that, the tailgate was slowly lowered until the flow depth reached the considered flow depth (5 cm) downstream of the main channel (see Figure 3.24). This instant was considered as the beginning of the experiments (t=0) and sediment feeders were turned on at that point. The experiments took 15 hours in total after this instant.

Figure 3.24: Adjusted flow depth downstream of the channel

Bed topography was systematically recorded during the experiments t=3 h, t=9 h, and at the end of the experiment (t=15 h) by using the distance measurement features of the Vectrino. Since the Vectrino needs to be slightly submerged in water for measuring, the water level was increased by raising the downstream tailgate and the sediment transport was stopped by decreasing the flow velocity. Also, the sediment feeders were switched off. Under these conditions, the bed topography was measured. Topography measurements were made at 10 cm apart for x and y axis along the main channel, and at 25 cm apart in tributaries.

Bed topography was not only obtained at the end of the experiment but the time evolution of bed topography was also investigated.

The water surface was measured just before stopping the experiment (t=15 h) by using ULS-40D probes. Water surface measurements were made at 25 cm apart for

x-axis along the main channel and the probes are placed at y=-50 cm, at y=0, and at y=50 cm. Water surface measurements were made 25 cm apart in the middle of the tributaries.

To restart the experiment, the downstream water level was adjusted by lowering the tailgate, and the sediment feeders were turned on. The stop and re-start processes were shown not to affect the bed topography

At the end of the experiments, photographs are taken using a GoPro camera which shows the plan view bathymetry along the main channel.

Bed topography was obtained t=3 h, t=9 h, and at the end of the experiment (t=15 h) in the main channel. At the end of the experiments, flow depths were obtained at y=-100 cm, y=0 cm and y=100 cm in the main channel and in the middle of the tributaries. Also, the bed topographies were obtained in tributaries t=15 h.

Chapter 4

Experimental Results and Discussion

In this study, two experiments have been carried out in a symmetrical channel confluence to identify the effects of the amount of sediment load on morphology under clear water and live-bed conditions. In addition to the bed morphology at the end of the experiments, its time evolution was also obtained. In this chapter, the results of these experiments were presented.

Experiment 1 (E1), and Experiment 2 (E2) denote the experiments without sediment feeding and with sediment feeding, respectively.

4.1 Results of Experiment 1

Bed morphologies of E1 evolved after 3 hours, 9 hours, and 15 hours as in Figure 4.1. Although there was water in the channel, the bank-attached bars are clearly visible.

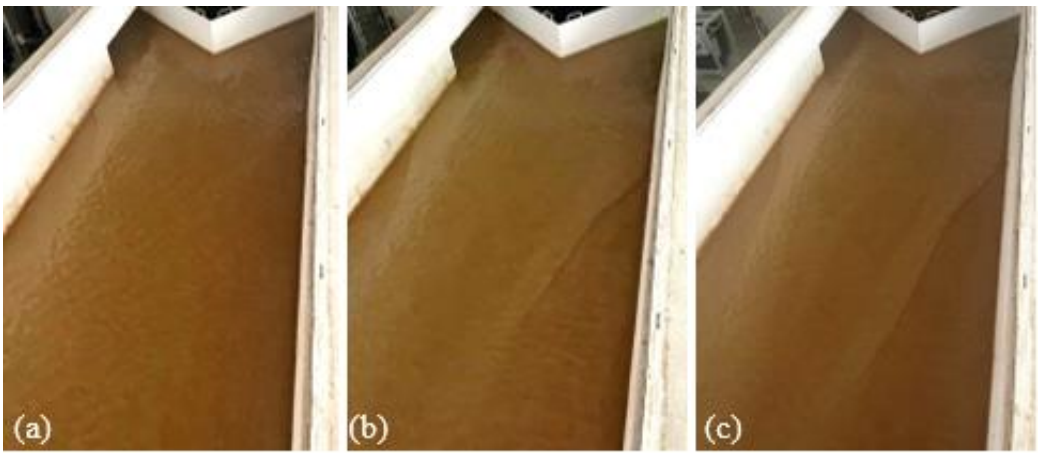

Figure 4.1: The view of bed morphology for E1 (a) 3 h, (b) 9 h, (c) 15 h

Figure 4.2 shows a three-dimensional illustration of bathymetries after 3 hours, 9 hours and 15 hours which are obtained using measured data.

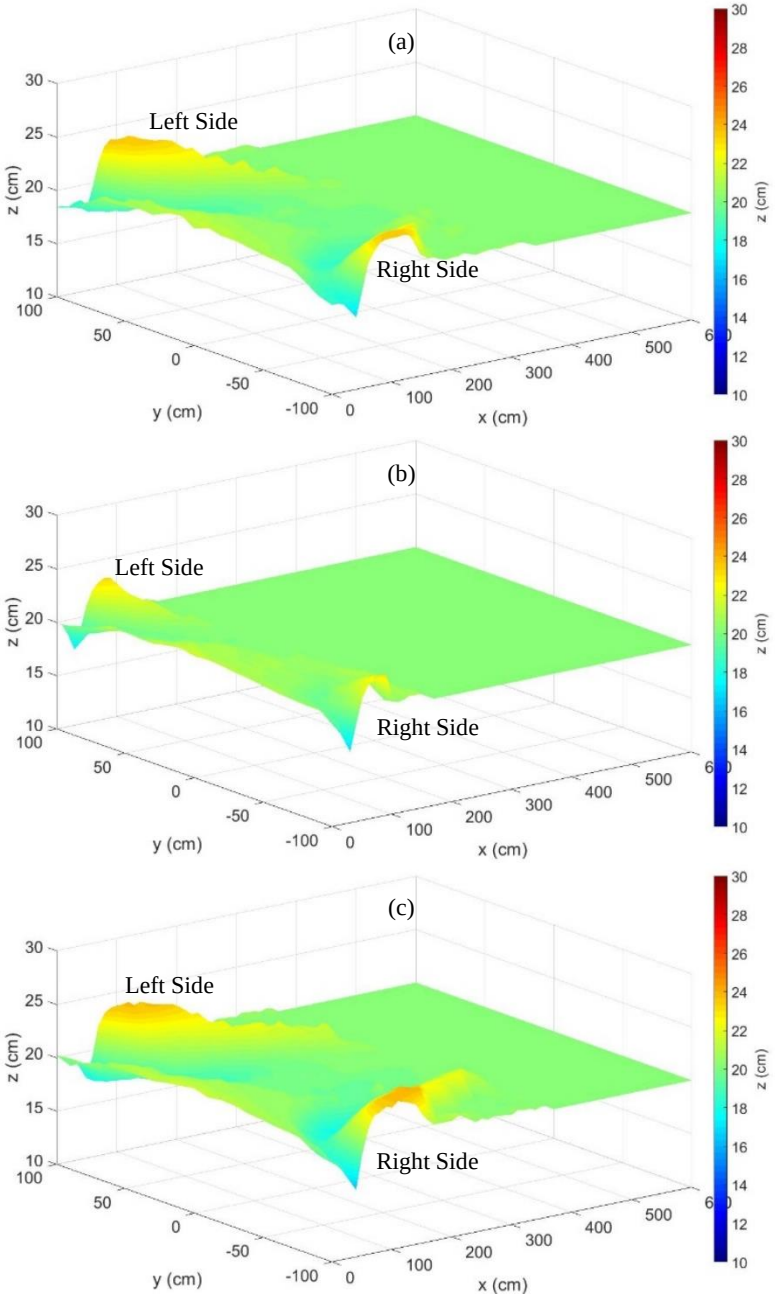

Figure 4.2: Three-dimensional bathymetry maps for E1 (a) 3 h, (b) 9 h, (c) 15 h

In order to see the time evolution of bed morphology more clearly, plan projections of the confluence morphologies after 3 hours, 9 hours, and 15 hours are given in Figure 4.3, covering the area defined by 0 m $\leq$ x $\leq$ 6 m and -1 m $\leq$ y $\leq$ 1 m.

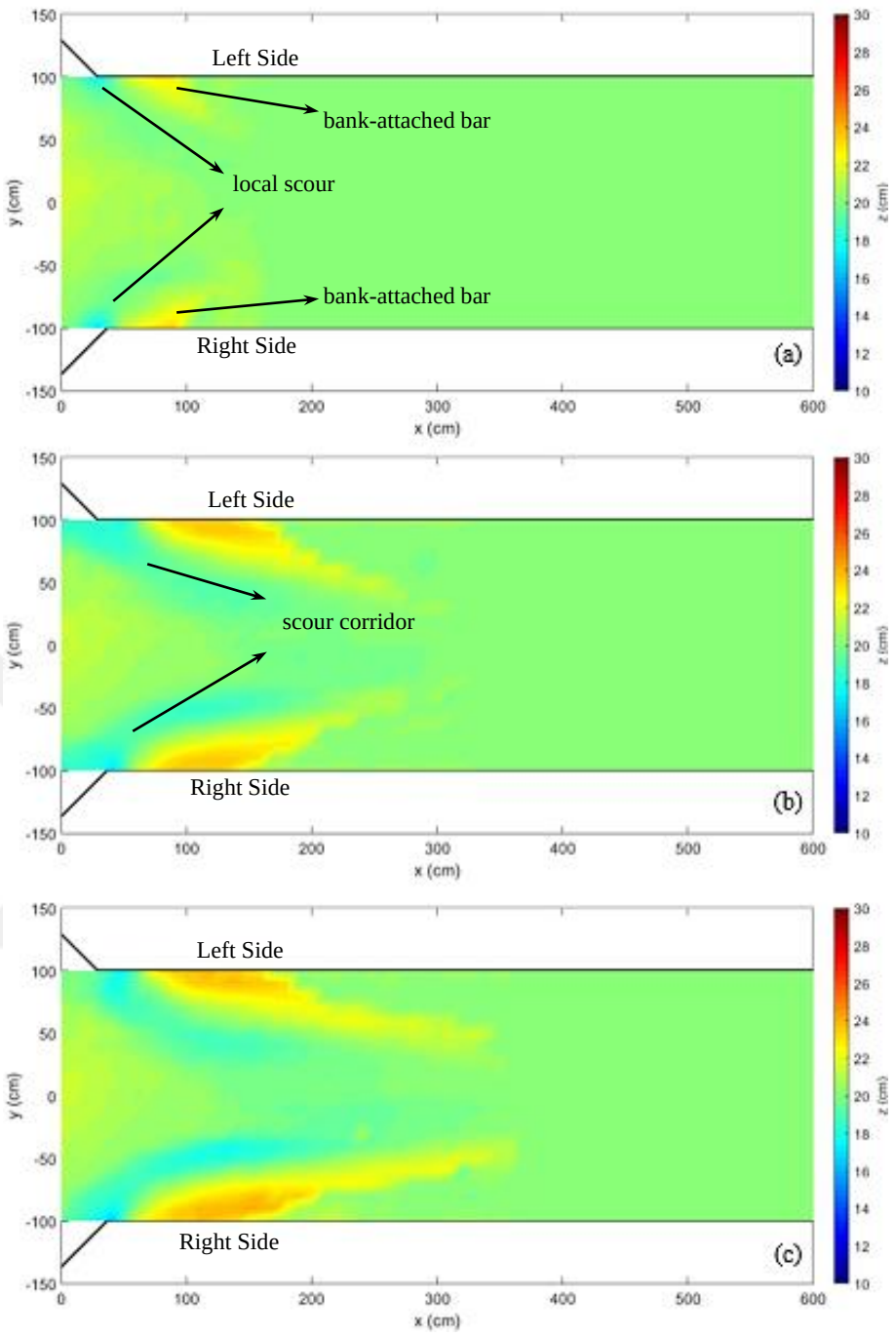

Figure 4.3: Evolution of the bed topography for E1 (a) 3 h, (b) 9 h, (c) 15 h

Local spots of scour were present at the downstream junction corners at all times as the bed morphology develops. Erosion was observed at the mouth of tributaries and this region expanded to downstream of confluence and scour corridors formed evidently after 3 hours. Depending on the deposition of transported sediment from the tributaries along the walls of the main channel downstream of the confluence, bank-attached bars began to develop and they expand in all three directions with time. There was no scour hole at the downstream of the confluence.

The average, minimum and maximum values of the bed elevations and their coordinates are given in Table 4.1.

Table 4.1: The average, minimum and maximum values of the bed elevations and coordinates for E1

z (cm)		t = 3 h	t = 9 h	t = 15 h
Left side	Average	20.49 cm	20.40 cm	20.53 cm
	Minimum (x,y)	17.10 cm (30 cm, 100 cm)	17.60 cm (50 cm, 100 cm)	17.70 cm (50cm, 100 cm)
	Maximum (x,y)	23.20 cm (80 cm, 100 cm)	23.70 cm (90 cm,100 cm)	23.90 cm (120 cm, 100 cm)
Right side	Average	20.57 cm	20.36 cm	20.48 cm
	Minimum (x,y)	16.70 cm (30, -100 cm)	16.80 cm (40 cm, -100 cm)	16.90 cm (40 cm,-100 cm)
	Maximum (x,y)	23.20 cm (80 cm, -100 cm)	23.60 cm (120 cm, -100 cm)	24.10 cm (150 cm,-90 cm)
All channel	Average	20.53 cm	20.38 cm	20.50 cm
	Minimum	16.70 cm	16.80 cm	16.90 cm
	Maximum	23.20 cm	23.70 cm	24.10 cm

Longitudinal profiles of the bed topography evolution at y=0 cm is shown in Figure 4.4. As seen in longitudinal bed topographies, there was no significant change in morphology in the middle of the main channel with time.

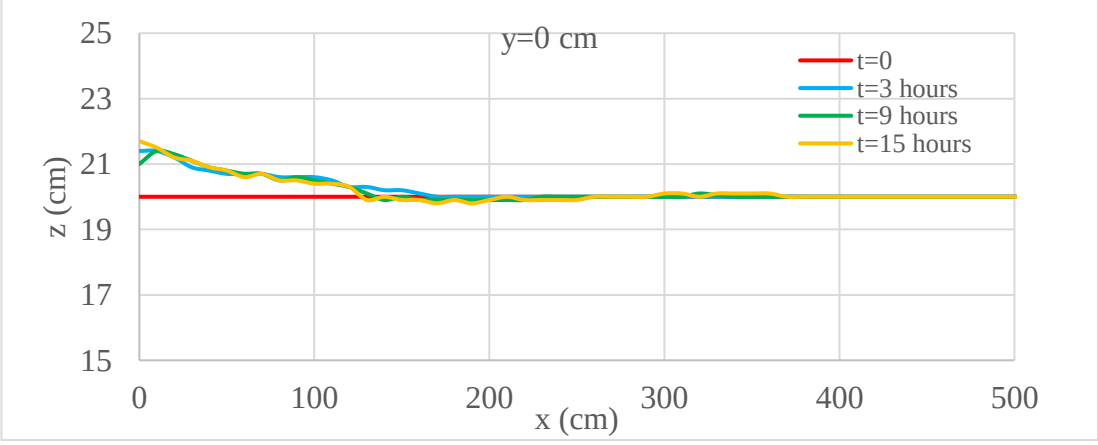

Figure 4.4: Longitudinal profiles of the bed topography at y=0 cm for E1

Longitudinal profiles of the bed topography evolution at y=-100 cm and y=100 cm are shown in Figure 4.5.

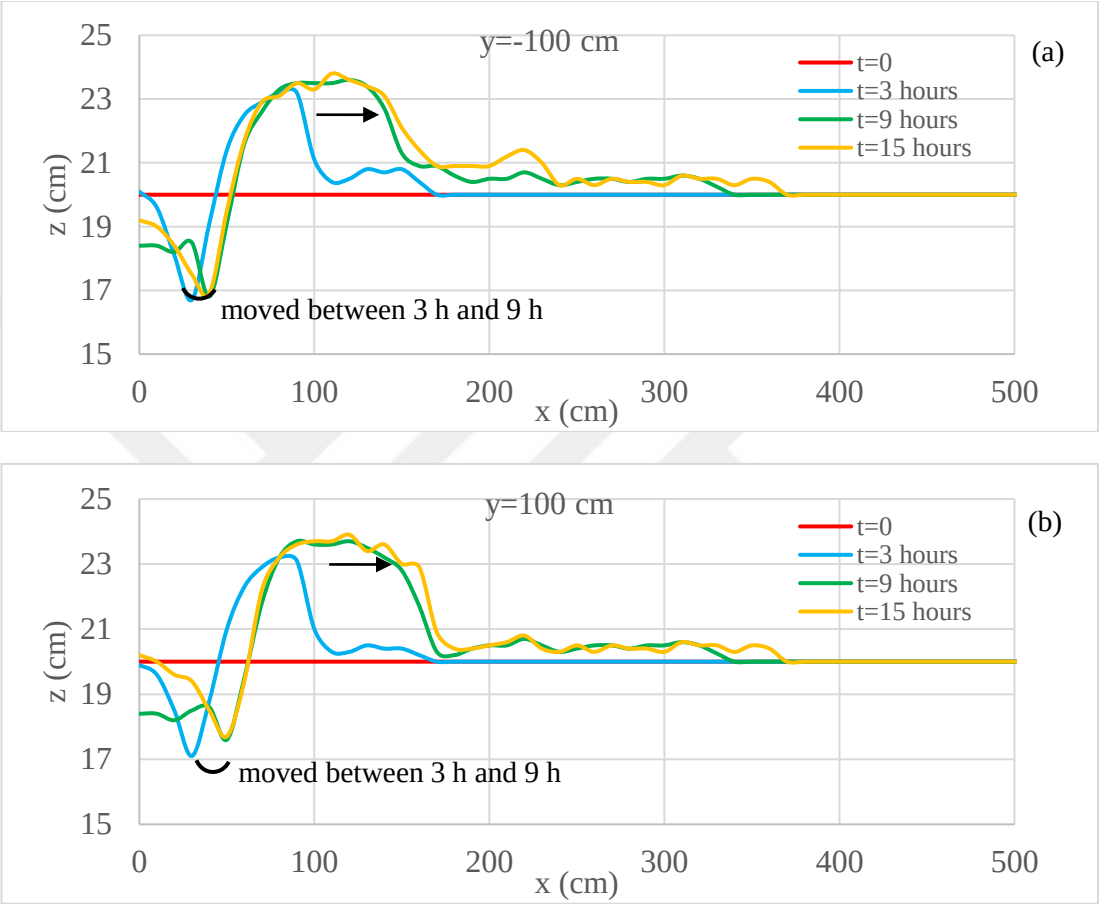

Figure 4.5: Longitudinal topography profiles (a) y=-100 cm, (b) y=100 cm for E1

For y=-100 cm and y=100 cm a scour and accumulation were observed at t=3 h and the scour moved downstream, and the accumulation zone expanded downstream between t=3 h and t=9 h. Then, bed profiles were the same between t=9 h and t=15 h.

Longitudinal profiles of the bed topography evolution at y=-50 cm and y=50 cm are shown in Figure 4.6.

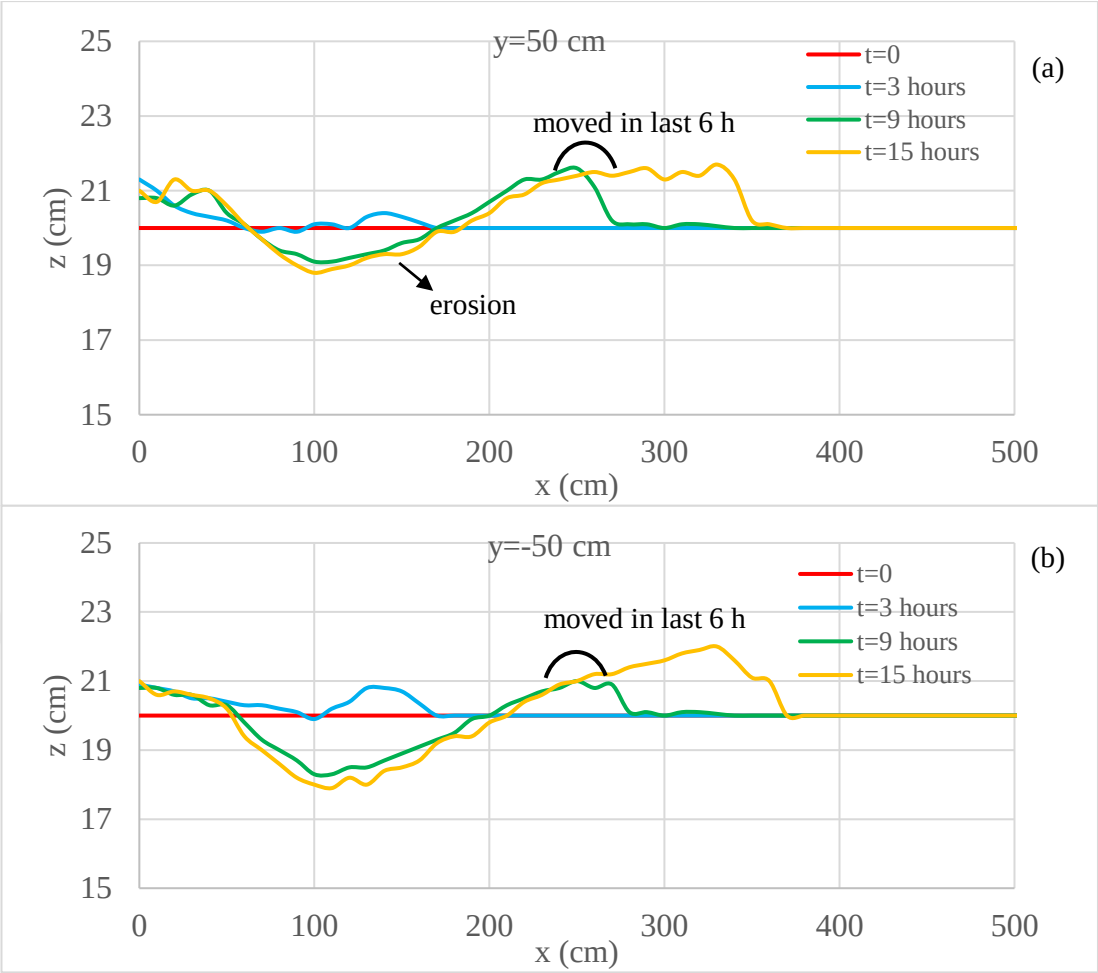

Figure 4.6: Longitudinal topography profiles (a) y=-50 cm, (b) y=50 cm for E1

For y=-50 cm and y=50 cm, there was no erosion t=3 h. As the expand of local scour, an erosion and an accumulation were observed at t=9 h, and the accumulation zone expanded downstream between t=9 h and t=15 h and no significant change was observed between t=9 h and t=15 h except the accumulation zone expanded downstream.

Table 4.2 shows the minimum and maximum values of the bed elevations and their coordinates for E1.

Table 4.2: The minimum and maximum values of the bed elevations at y=100 cm, y=-50 cm, y=0 cm, y=-50 cm and y=100 cm for E1

	z (cm) x (cm)	**y=100 cm**	**y=50 cm**	**y=0 cm**	**y=-50cm**	**y=-100 cm**
t=3 h	Minimum	17.1 cm 30 cm	19.7 cm 70 cm	No scour	19.9 cm 100 cm	16.7 cm 30 cm
	Maximum	23.9cm 120 cm	21.0 cm 10 cm	21.4 cm 0 cm	20.8 cm 130 cm	23.1 cm 80 cm
t=9 h	Minimum	17.7 cm 50 cm	19.1 cm 100 cm	No scour	18.3 cm 110 cm	16.8 cm 40 cm
	Maximum	23.6 cm 90 cm	21.6 cm 250 cm	21.4 10 cm	21.0 cm 250 cm	23.6 cm 120 cm
t=15 h	Minimum	17.7 cm 50 cm	18.8 cm 100 cm	No scour	17.9 cm 110 cm	16.9 cm 40 cm
	Maximum	23.9 cm 120 cm	21.7 cm 330 cm	21.7 0 cm	22.0 cm 330 cm	23.8 110 cm

The rate of change in bed elevation (dz/dt) was calculated by dividing the change in elevation between two consecutive measurements by the time interval. The rates of change in bed elevations are shown in Figure 4.7.

The pink-colored area represents where the rates of change in bed elevation were 0 cm/h. The rates of change in bed elevations were between -1.10 cm/h and 1.07 cm/h and their average was obtained 0.18 cm/h in the first 3 hours of the experiment. The maximum and minimum values of rates of change in bed elevations were 0.57 cm/h and -0.57 cm/h and their average was -0.014 cm/h between 3 hours and 9 hours. Finally, the rates of change in bed elevations were between -0.2 cm/h and 0.3 cm/h and their average was obtained 0.008 cm/h in the last 6 hours of the experiment. According to the results, the rates of change in bed elevations decreased and the area of pink-colored increased with time.

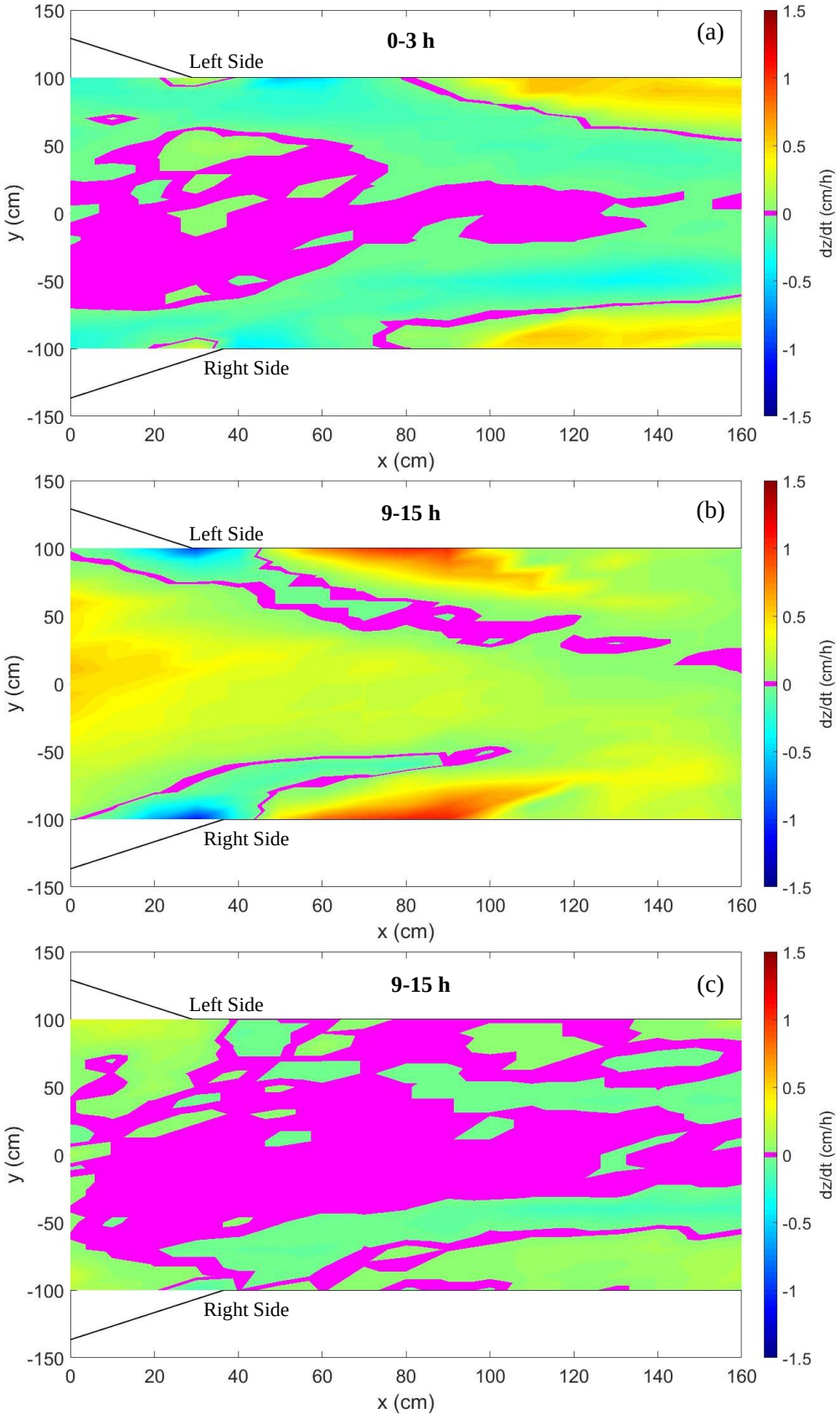

Figure 4.7: The bed elevation change rates for E1 (a) 0-3 h, (b) 3-9 h, (c) 9-15 h

Figure 4.8 presents the longitudinal profiles of bed morphologies and flow depths at y=50 cm, y=0 cm and y=-50 cm with the initial bed at the end of the experiment. Also, the flow depths at x=4 m, and x=6 m are shown in Figure 3.8. S_0 was calculated as 0.00175 according to formulas of Ackers and White [19]. The slope of water surface (S_w) at y=0 cm was smaller than S_0.

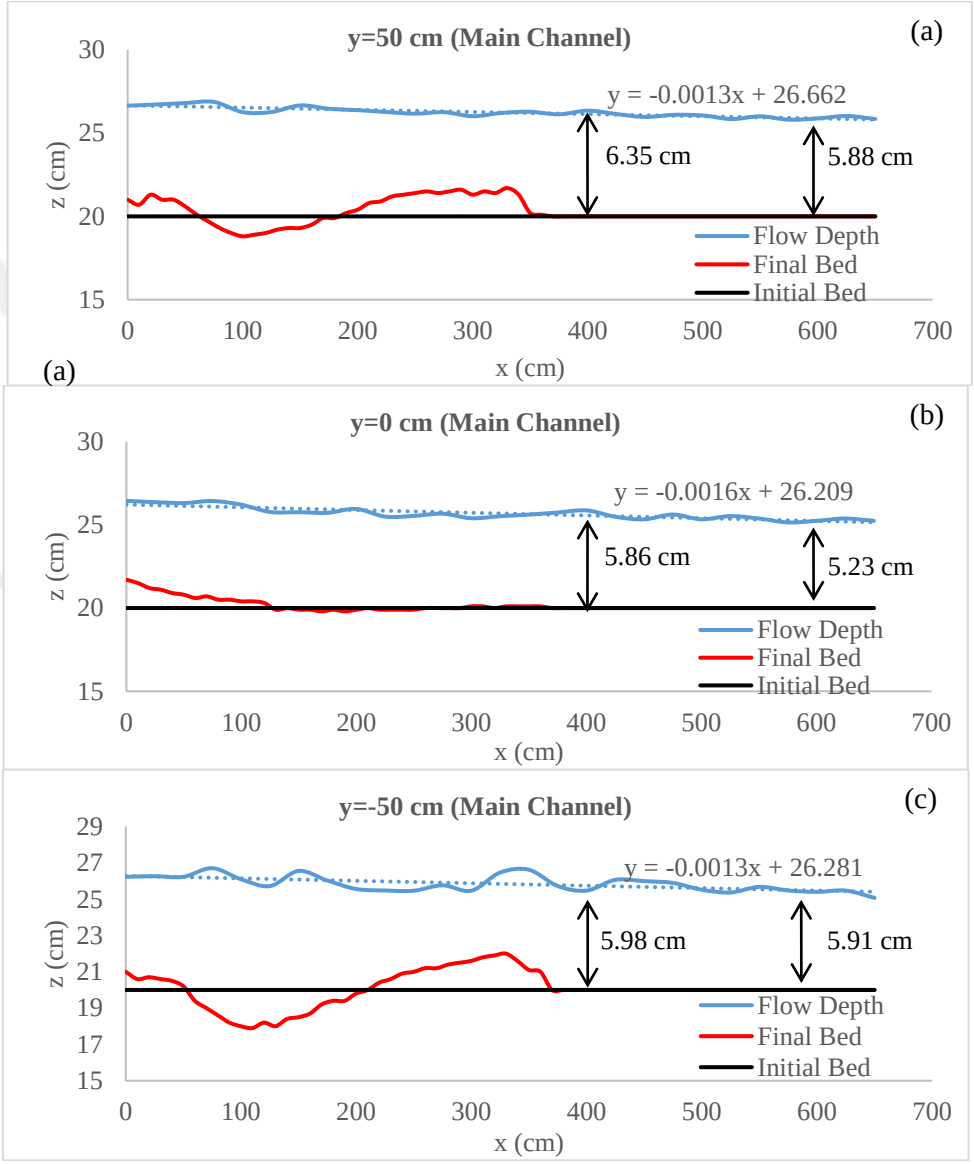

Figure 4.8: Final longitudinal profiles of flow depth and bed morphology for E1 (a) y=50 cm, (b) y=0 cm, (c) y=-50 cm

The final flow depths and the bed morphologies in the middle of the tributaries are shown in Figure 4.9.

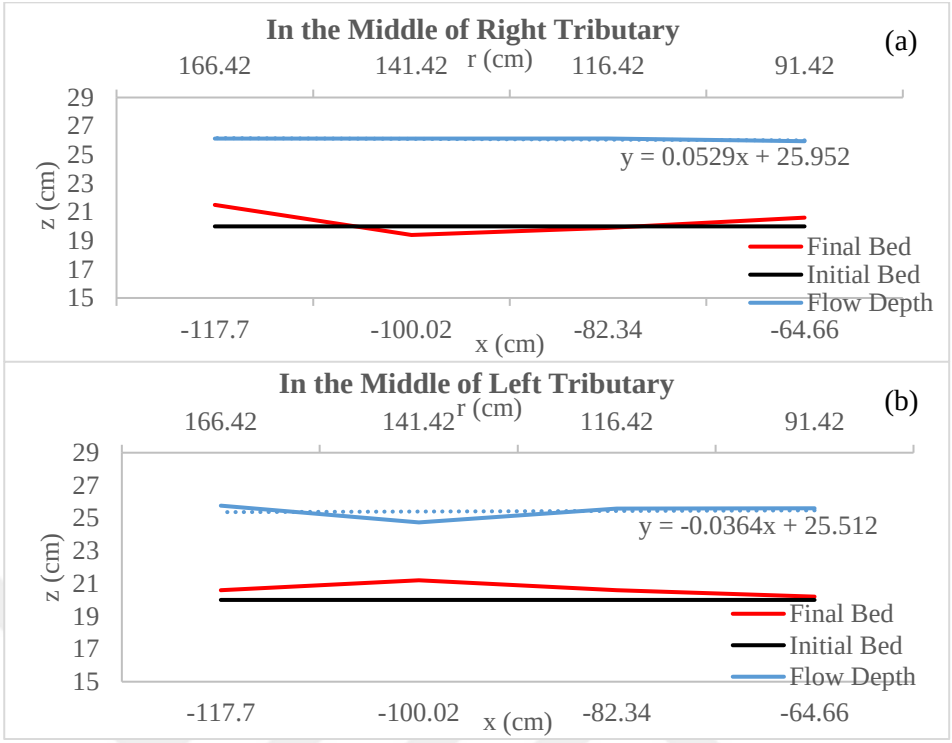

Figure 4.9: Final flow depth and bed morphology in tributaries for E1 (a) Right, (b) Left

4.2 Results of Experiment 2

Bed morphologies of E2 evolved after 3 hours, 9 hours, and 15 hours as in Figure 4.10. Although there was water in the channel, the bank-attached bars are clearly visible.

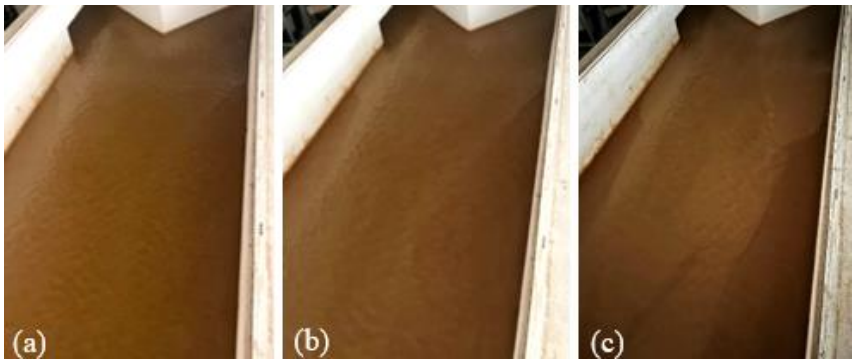

Figure 4.10: The view of bed morphology for E2 (a) 3 h, (b) 9 h, (c) 15 h

Figure 4.11 shows a three-dimensional illustration of bathymetries after 3 hours, 9 hours, and 15 hours which are obtained using measured data.

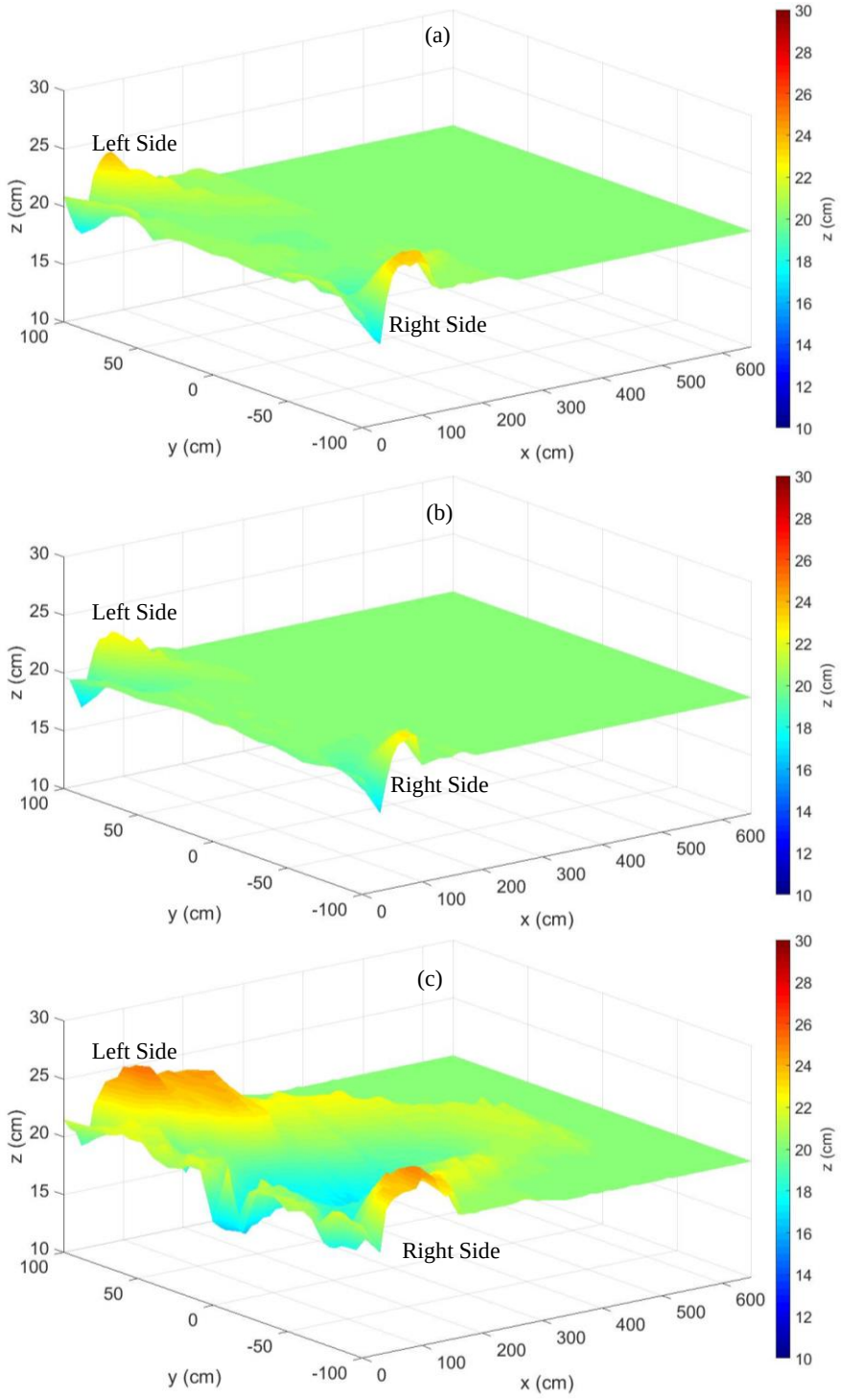

Figure 4.11: Three-dimensional bathymetry maps for E2 (a) 3 h, (b) 9 h, (c) 15 h

In order to see the time evolution of bed morphology more clearly, plan projections of the confluence morphologies after 3 hours, 9 hours, and 15 hours are given in Figure 4.12, covering the area defined by $0 \leq x \leq 6$ m and -1 m $\leq y \leq 1$ m.

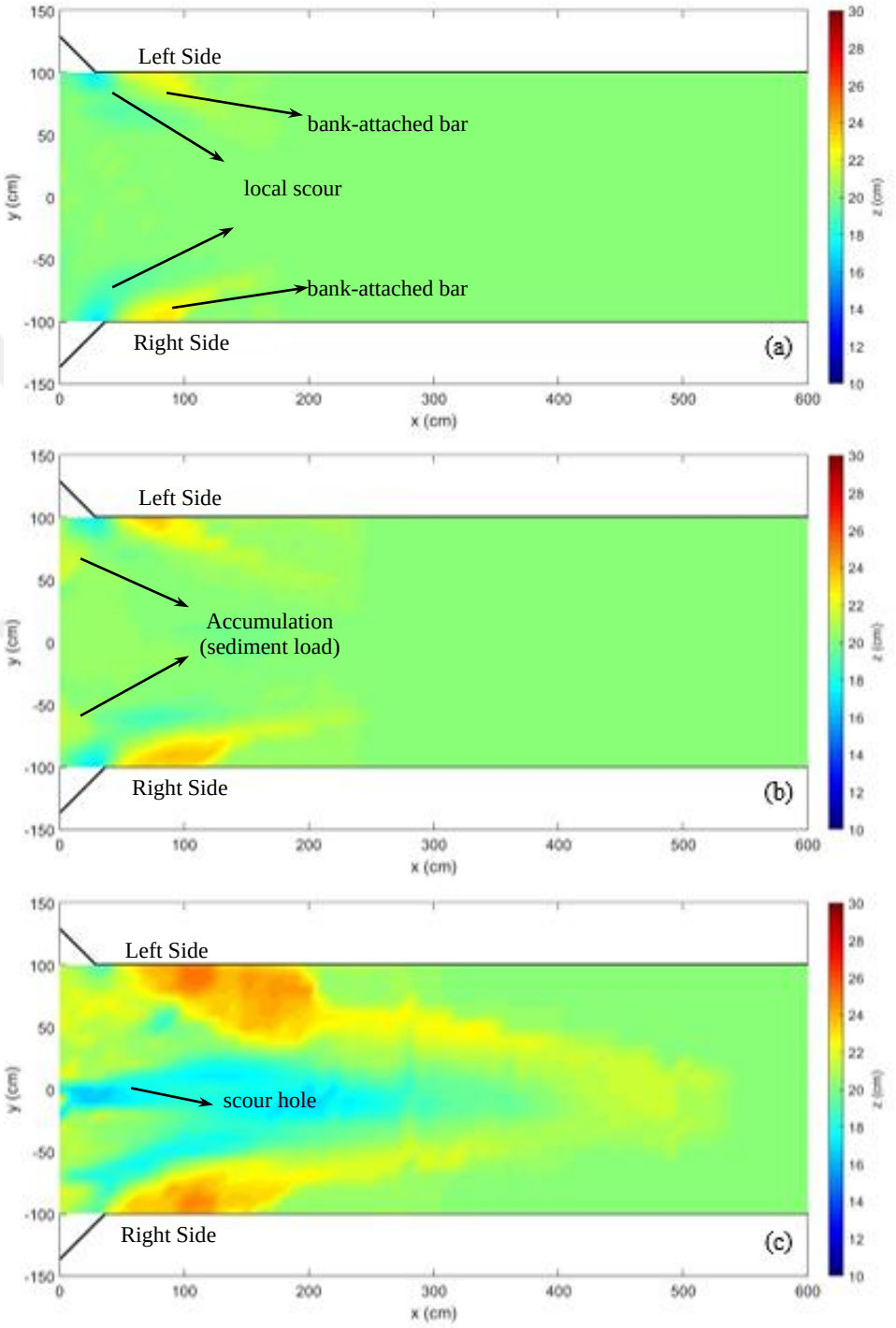

Figure 4.12: Evolution of the bed topography for E2 (a) 3 h, (b) 9 h, (c) 15 h

Local spots of scour were present at the downstream junction corners at all times as the bed morphology develops. The erosion in the mouth of tributaries cause the presence of bank-attached bars which were observed along the walls of the main channel and there was no sediment load and the scour hole in the main channel t=3 h.

After 9 hours, the sediment load from the tributaries reached the main channel and they prevented to develop of erosion in the tributary mouths. As time goes, it was observed that larger, higher and wider bank-attached bars. A scour hole didn't form yet t=9 h.

At the end of the experiment, a scour hole formed at the confluence (t=15 h).

The average, minimum and maximum values of the bed elevations and their coordinates are given in Table 4.3.

Table 4.3: The average, minimum and maximum values of the bed elevations and coordinates for E2

z (cm)		**t = 3 h**	**t = 9 h**	**t = 15 h**
Left side	Average	20.25 cm	20.52 cm	21.15 cm
	Minimum (x,y)	16.70 cm (30 cm, 100 cm)	17.30 cm (30 cm, 100 cm)	17.10 cm (130 cm, 10 cm)
	Maximum (x,y)	22.70 cm (80 cm, 100 cm)	23.90 cm (80 cm, 100 cm)	25.30 cm (100 cm, 90 cm)
Right side	Average	20.23 cm	20.51 cm	20.37 cm
	Minimum (x,y)	16.70 cm (30 cm, -100 cm)	17.00 cm (30 cm, -100 cm)	16.00 cm (40 cm,-80 cm)
	Maximum (x,y)	22.90 cm (80 cm, -100 cm)	23.80 cm (90 cm, -90 cm)	24.7 cm (80 cm,-80 cm)
All channel	Average	20.24 cm	20.51 cm	20.76 cm
	Minimum	16.70 cm	17.00 cm	16.00 cm
	Maximum	22.90 cm	23.90 cm	25.30 cm

Longitudinal profiles of the bed topography evolution at y=0 cm is shown in Figure 4.13 and at y=-100 cm and y=100 cm are shown in Figure 4.14.

As seen in longitudinal profiles of bed topographies, while it was not observed a scour zone t=3 h and t=9 h, an erosion and evident accumulation occurred at the end of the experiment at y=0 cm.

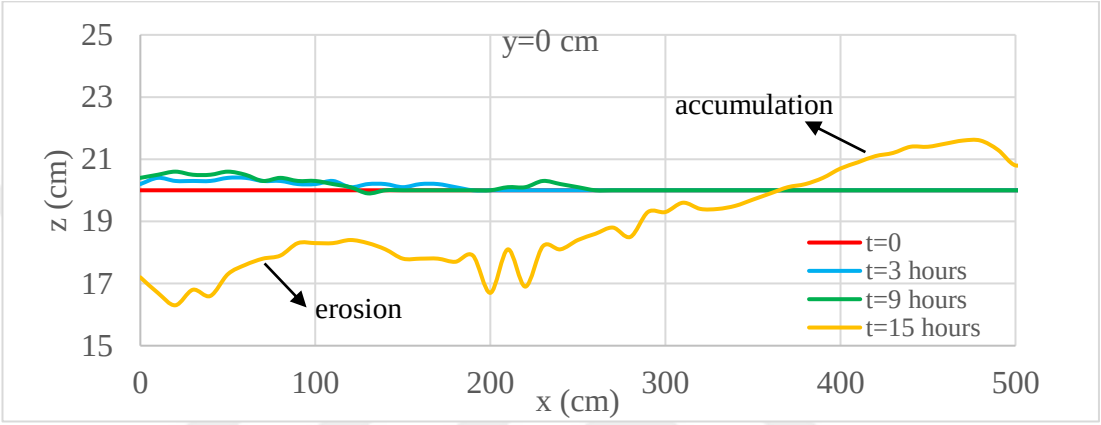

Figure 4.13: Longitudinal profiles of the bed topography at y=0 cm for E2

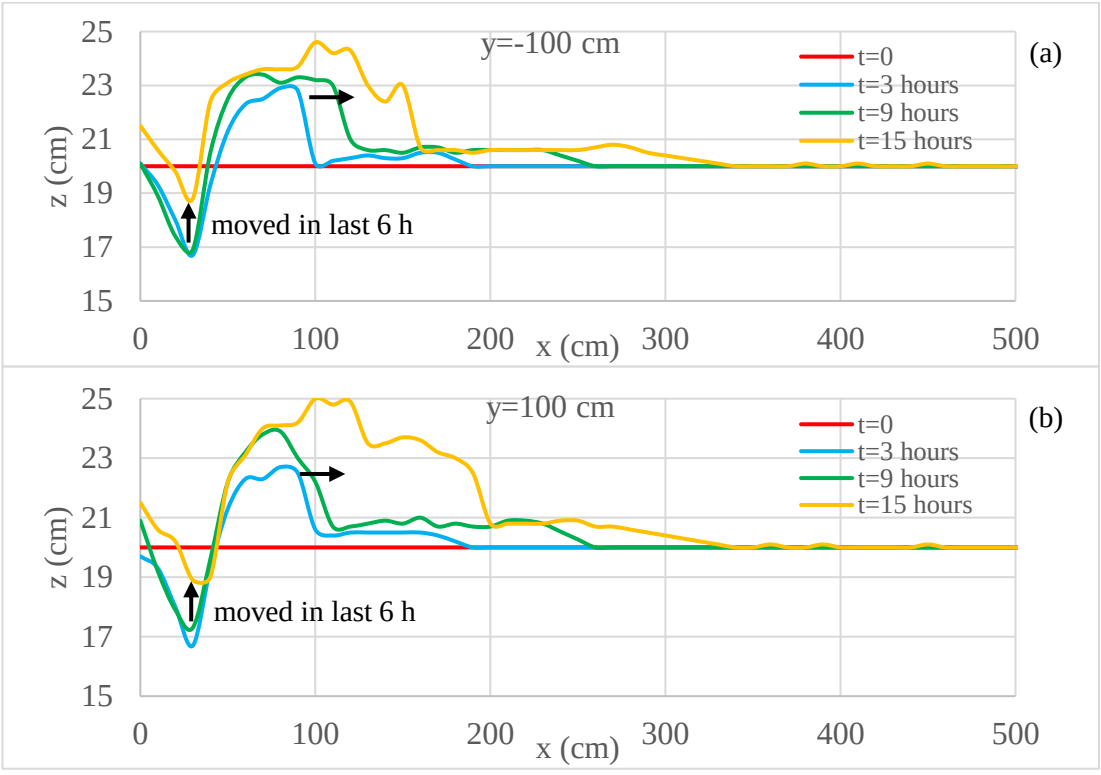

Figure 4.14: Longitudinal topography profiles (a) y=-100 cm, (b) y=100 cm for E2

According to Figure 4.13, a scour and accumulation were observed t=3 h. With the sediment load reaching the main channel, the depth of this scour decreased between t=9 h and t=15 h. The bank-attached bar expanded in the x and z direction in with time at y=-100 cm and y=100 cm.

Longitudinal profiles of the bed topography evolution at y=-50 cm and y=50 cm are shown in Figure 4.15.

For y=-50 cm and y=50 cm, while there was no evident scour t=3 h and t=9 h, a scour and an accumulation occurred at the end of the experiment.

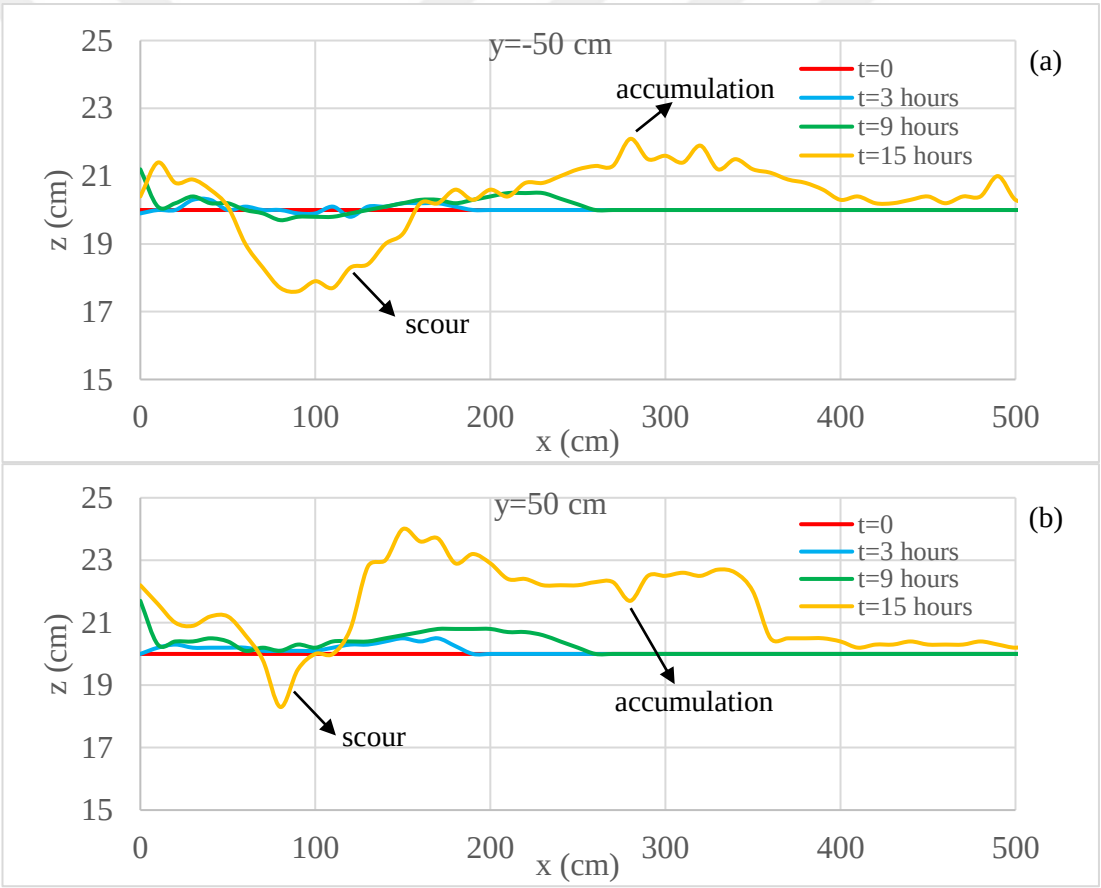

Figure 4.15: Longitudinal topography profiles (a) y=-50 cm, (b) y=50 cm for E2

Table 4.4 shows the minimum and maximum values of the bed elevations and their coordinates for E2.

Table 4.4: The minimum and maximum values of the bed elevations at y=100 cm, y=-50 cm, y=0 cm, y=-50 cm and y=100 cm for E2

	z (cm) x (cm)	**y=-100 cm**	**y=50 cm**	**y=0 cm**	**y=-50cm**	**y=100 cm**
t=3 h	Minimum	16.7 cm 30 cm	No scour	No scour	No scour	16.7 cm 30 cm
	Maximum	23.3 cm 90 cm	21.7 cm 0 cm	20.5 cm 10 cm	20.3 cm 30 cm	22.7 cm 80 cm
t=9 h	Minimum	16.9 cm 30 cm	No scour	No scour	No scour	17.3 cm 30 cm
	Maximum	23.4 cm 60 cm	20.6 cm 150 cm	20.6 cm 20 cm	20.4 cm 30 cm	24.2 cm 80 cm
t=15 h	Minimum	18.8 cm 30 cm	18.3 cm 80 cm	16.3 cm 20 cm	17.6 cm 90 cm	19.0 cm 40 cm
	Maximum	24.6 cm 100 cm	24.0 cm 150 cm	21.6 cm 480 cm	22.1 cm 280 cm	25.0 cm 100 cm

The rate of change in bed elevations are shown in Figure 4.16. The pink-colored area represents where the rate of change in bed elevations was 0 cm/h. The bed rate of change in bed elevations was between -1.23 cm/h and 0.96 cm/h and their average was 0.08 cm/h in the first 3 hours of the experiment. The maximum and minimum values of the rate of change in bed elevations were 0.6 cm/h and -0.15 cm/h and their average was 0.05 cm/h between 3 hours and 9 hours. The rate of change in bed elevations was between -0.7 cm/h and 0.8 cm/h and their average was obtained as 0.06 cm/h in the last 6 hours of the experiment.

The rate of change in bed elevations decreased and the pink-colored area increased until 9 hours. Then, the rate of change in bed elevations increased in the last 6 hours depending on the sediment load.

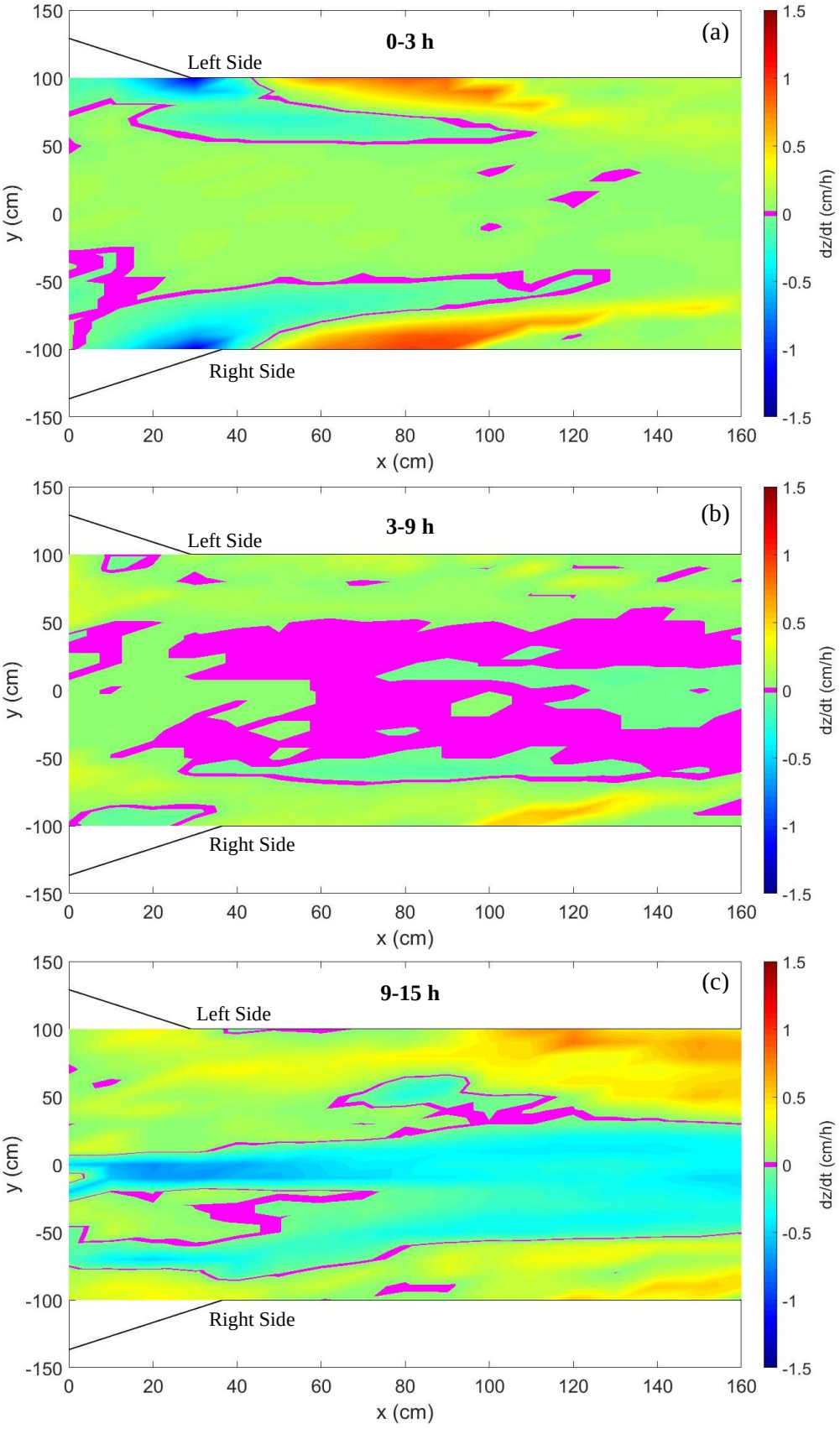

Figure 4.16: The bed elevation change rates for E2 (a) 0-3 h, (b) 3-9 h, (c) 9-15 h

Figure 4.17 presents the longitudinal profiles of bed morphologies and flow depths at y=50 cm, y=0 cm and y=-50 cm with the initial bed at the end of the experiment.

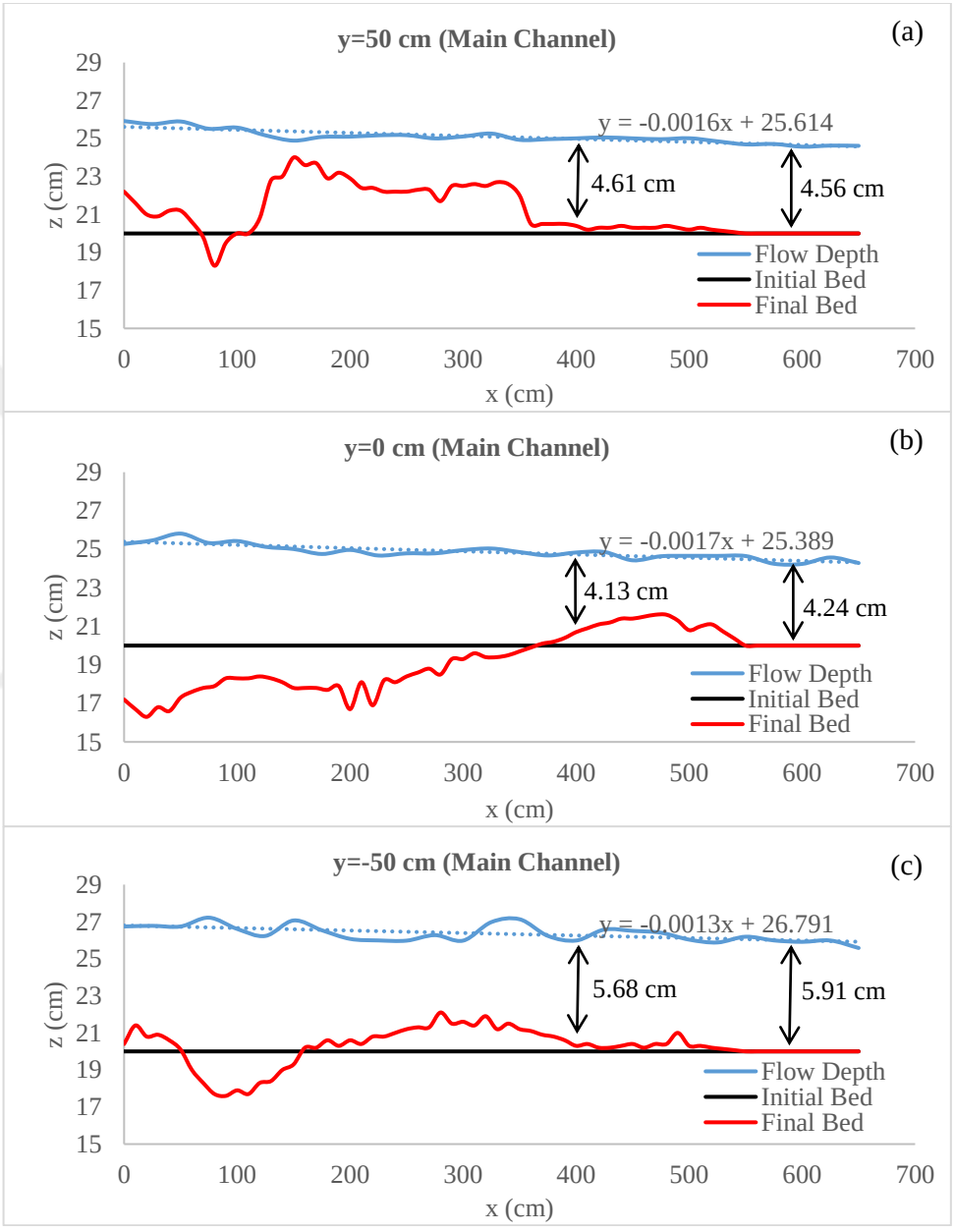

Figure 4.17: Final longitudinal profiles of flow depth and bed morphology for E2 (a) y=50 cm, (b) y=0 cm, (c) y=-50 cm

S_0 was calculated as 0.00175 according to formulas of Ackers and White [19].The slope of water surface (S_w) at y=0 cm was 0.0017 and S_0 and S_w are compatible.

The final flow depths and the bed morphologies in the middle of the tributaries are shown in Figure 4.18.

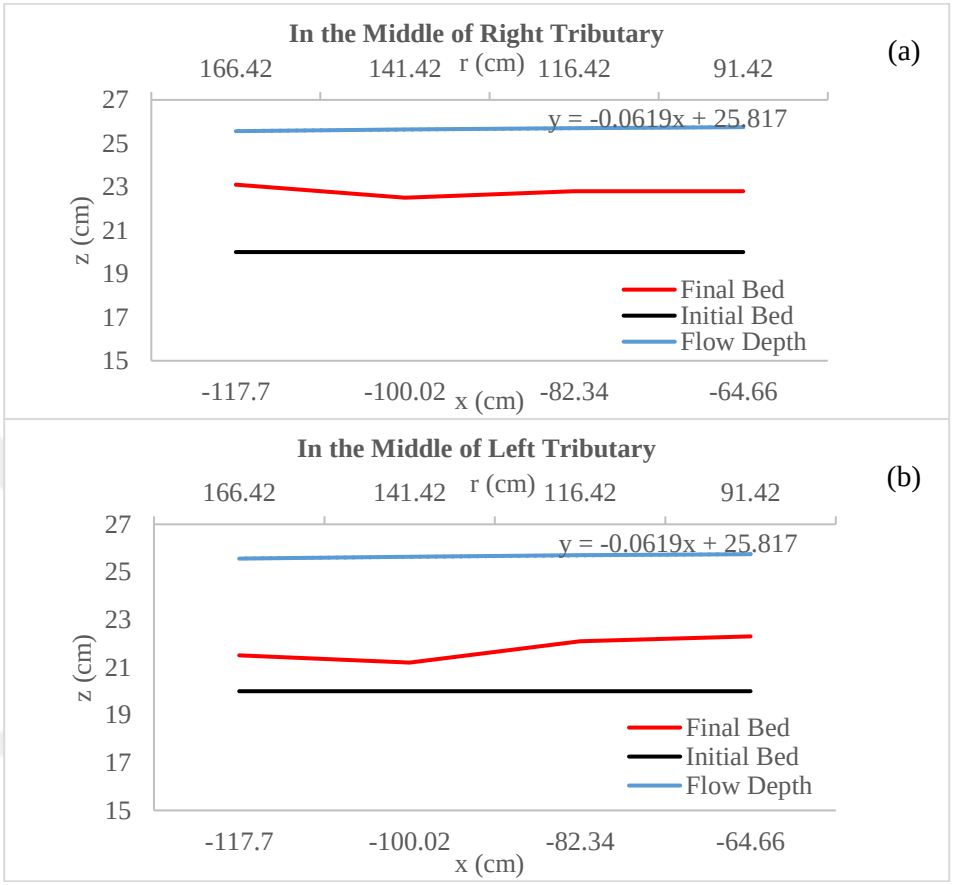

Figure 4.18: Final flow depth and bed morphology in tributaries for E1 (a) Right, (b) Left

3.3 Comparison of the Final State of the Experiments

The bed morphologies t=3 h were the same for both experiments. Because the effects of the sediment load didn't reach the main channel.

While a scour corridor formed in E1, the sediment load from the tributaries prevented to develop erosion in the tributary mouths and it wasn't observed a scour corridor after 9 hours in E2.

The values of the rate of change in bed elevations showed that the bed morphologies t=9 h and t=15 h were almost the same in E1, and the rate of change in bed elevations increased between t=9 h and t=15 h in E2.

The bed topographies for all channels and the plan views of the main channel are shown in Figure 4.19 and Figure 4.20.

As seen in Figure 4.19 and Figure 4.20, the bed elevations in the tributaries were higher with sediment feeding.

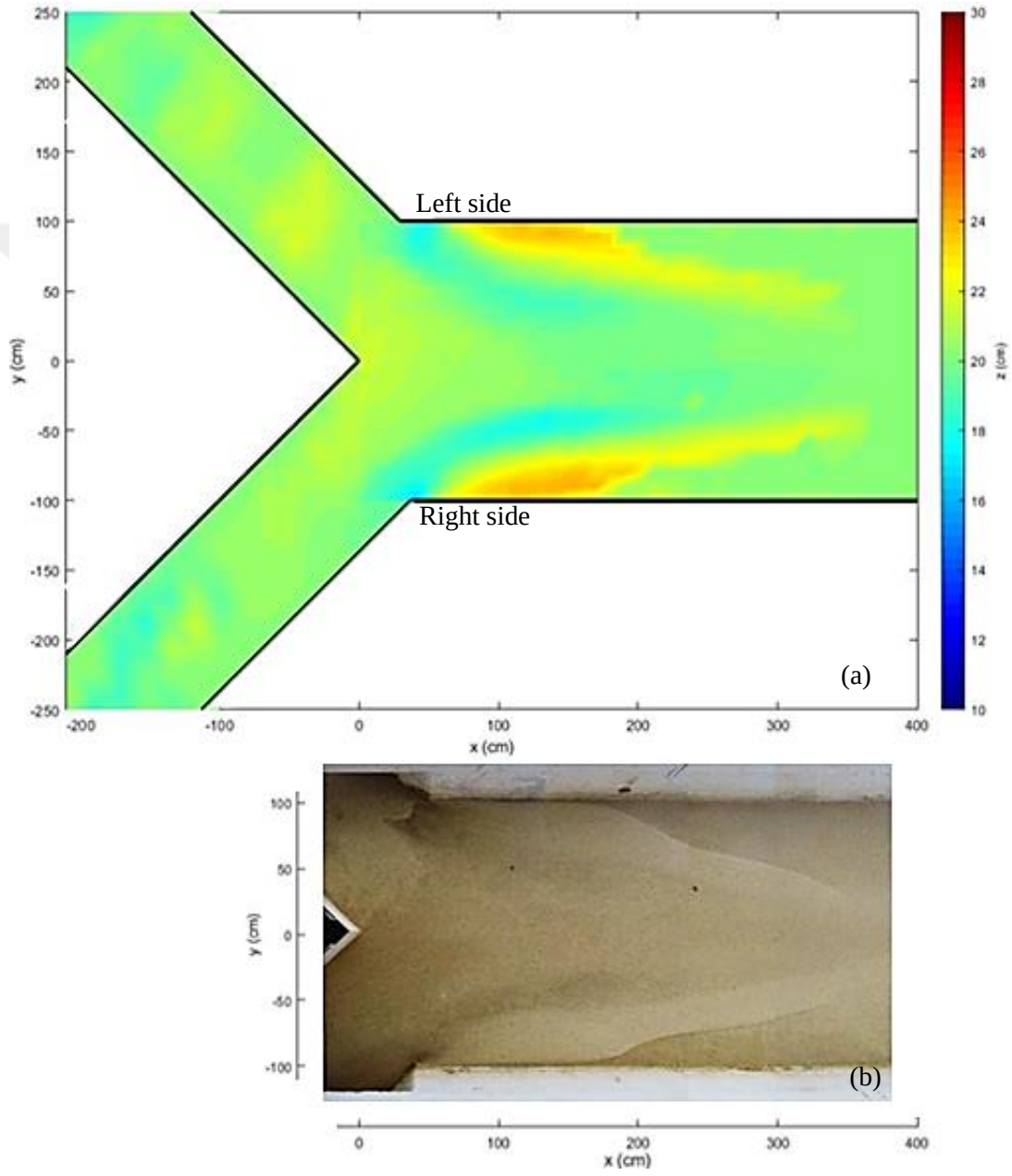

Figure 4.19: E1 (a) The bed topographies, (b) The plan view

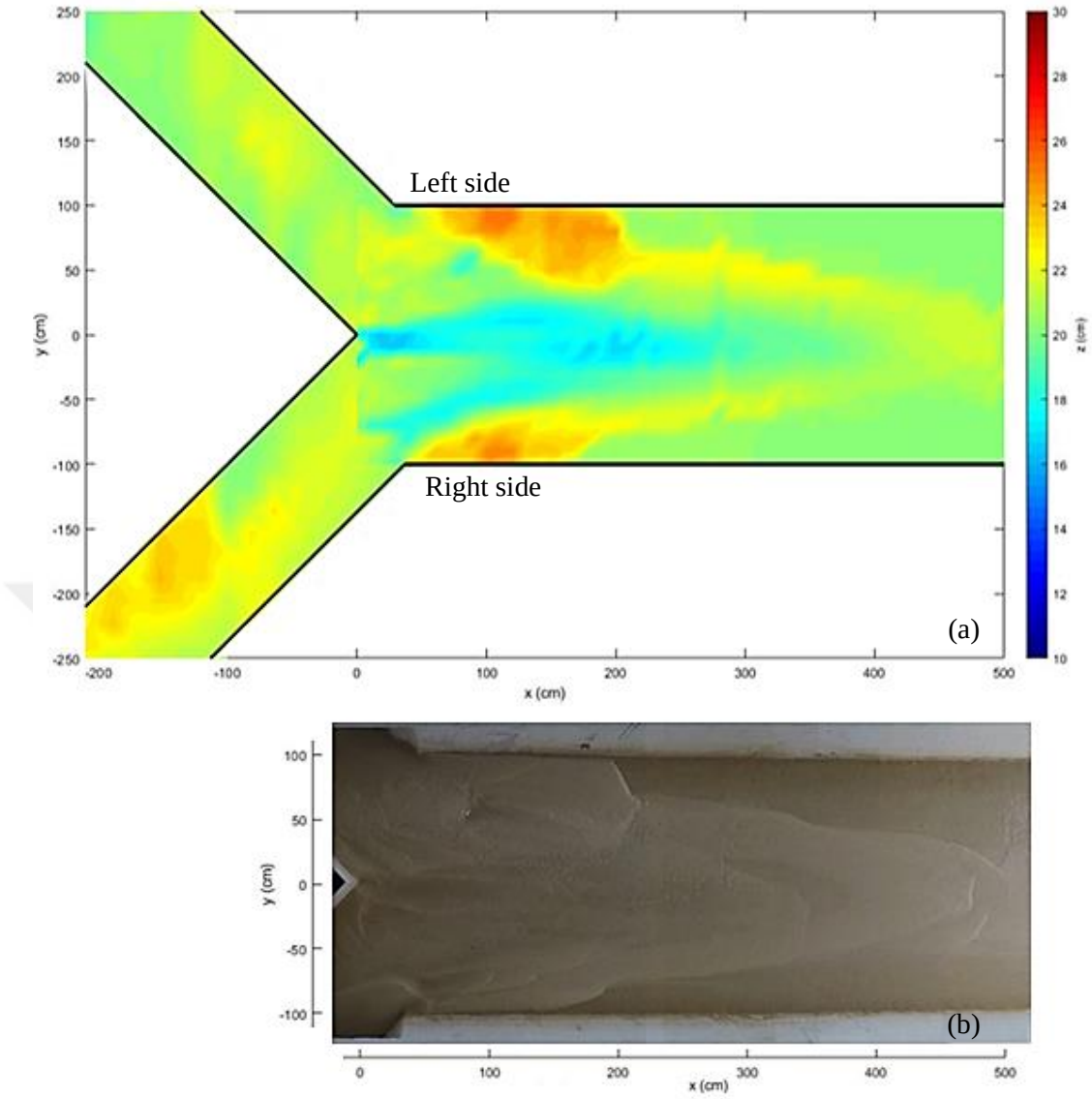

Figure 4.20: E2 (a) The bed topographies, (b) The plan view

Depending on the amount of sediment load, larger, higher, and wider bank-attached bars were observed at the end of the E2.

While no scour hole was formed in E1, according to the effect of the sediment load, a scour hole was observed at the end of E2.

Chapter 5

Conclusions

In this study, two experiments were carried out on the open channel confluence in İzmir Katip Çelebi University Hydraulics Laboratory, where two symmetrical side tributaries are connected to the main channel at an angle of 90˚**.** This study aims to identify the effects of sediment load on the time evolution of the morphology of a large-scale laboratory movable-bed symmetrical confluence. While the flow rate from the tributaries is equal and 20 l/s for both experiments, the amount of sediment loads was different and set as 0 kg/min and 0.1 kg/min for E1 and E2, respectively. The flow depth at downstream of the confluence with the cover at the downstream of the experimental set-up was adjusted to be 5 cm. The same conditions were maintained for three different periods of 3 hours, 9 hours, and 15 hours, and at the end of each period, the experiment was paused to obtain the bed elevations.

Bed topography was not only obtained at the end of the experiment but the time evolution of bed topography was also investigated.

In this chapter, the findings of this study are listed below.

For the E1;

- Maximum bed elevation of the bank-attached bar was 23.2 cm t=3 h.
- Maximum bed elevation of the bank-attached bar was 23.7 cm t=9 h.
- Maximum bed elevation of the bank-attached bar was 24.1 cm t=15 h.
- Minimum bed elevation of local scour at the downstream corner of the confluence was 16.7 cm t=3 h.
- Minimum bed elevation of scour corridor was 18.4 cm t=9 h.

- Minimum bed elevation of scour corridor was 17.8 cm t=9 h.
- There was no scour hole at the confluence.
- The water surface slopes were calculated as -0.0013, -0.0016, and -0.0013 at y=50 cm, y=0 cm, and y=-50 cm of the main channel t=15, respectively.
- The water surface slopes were calculated as 0.05, and -0.03 in the middle of the right and left tributaries t=15, respectively.

For the E2;

- Maximum bed elevation of the bank-attached bar was 22.9 cm t=3 h.
- Maximum bed elevation of the bank-attached bar was 23.9 cm t=9 h.
- Maximum bed elevation of the bank-attached bar was 25.3cm t=15 h.
- Minimum bed elevation of local scour at the downstream corner of the confluence was 16.7 cm t=3 h.
- Minimum bed elevation of scour corridor was 18.4 cm t=9 h.
- There was no scour corridor depending on the sediment load in the tributaries.
- At the end of the E2, a scour hole was observed, and the scour depth was 4 cm.
- The water surface slopes were calculated as -0.0016, -0.0017, and -0.0013 at y=50 cm, y=0 cm, and y=-50 cm of the main channel t=15, respectively.
- The water surface slopes were calculated as -0.06, and -0.06 in the middle of the right and left tributaries t=15, respectively.

Depending on the amount of sediment load, larger, higher, and wider bank-attached bars were observed at the end of the E2. The maximum bed elevation of the bank-attached bar in E1 was 1.2 cm higher than in E2 at the end of the experiments.

While no scour hole was formed in E1, according to the effect of the sediment load, a scour hole was observed at the end of E2.

In further studies:

- Effects of flow rate on bed morphology of symmetrical confluence can be examined by performing experiments under different discharge conditions,

- The bed topography can be obtained, and results may be compared for the cases with higher sediment feeding amounts in the tributaries,
- The duration of the experiment may be extended until the equilibrium condition is reached.

References

[1] Bombar G, Cardoso AH. Effect of the sediment discharge on the equilibrium bed morphology of movable bed open-channel confluences. Geomorphology 2020; 367.

[2] Asymmetrical River Confluence [İnternet]. [17.12.2022]. https://en.wikipedia.org/wiki/Confluence.

[3] Symmetrical River Confluence [İnternet]. [17.12.2022]. https://stock.adobe.com/search?k=river+confluence&asset_id=213621284.

[4] Constantinescu G, Miyawaki S, Rhoads B, Sukhodolov A. Numerical analysis of the effect of momentum ratio on the dynamics and sediment-entrainment capacity of coherent flow structures at a stream confluence. Journal of Geophysical Research 2012; 117(F4028). doi.org/10.1029/2012JF002452.

[5] Ghobadian R, Shafai Bajestan M. Investigation of sediment patterns at river confluence. Journal of Applied Sciences 2007; 7(10): 1372-1380.

[6] Ezcurra de Drago I, Marchese M, Montalto L. Benthic invertebrates. Ed.: Iriondo MH, Paggi JC, Parma MJ. In TheMiddle Paran´a River: Limnology of a Subtropical Wetland.. Springer; 2007. 251–275.

[7] Ashmore P, Parker G. Confluence scour in coarse braided streams. Geography Publications 1983; 295.

[8] Best JL. Flow dynamics at river channel confluences: Implications for sediment transport and bed morphology. Special Publications of SEPM, Recent Developments in Fluvial Sedimentology (SP39) 1987; 27-35.

[9] Biron P, Best JL, Roy AG. Effects of bed discordance on flow dynamics at open channel confluences. Journal of Hydraulic Engineering 1996; 122(12): 676–682.

[10] Mosley MP. An experimental study of channel confluences. The Journal of Geology 1976; 84(5); 535–562.

[11] Guillén-Ludena S. Hydro-morphodynamics of open-channel confluences with low discharge ratio and dominant tributary sediment supply (doctoral thesis). Portugal: Instituto Superior Técnico, Da Universidade de Lisboa; 2015.

[12] Shields A. Application of similarity principles and turbulence research to bed-load movement. California Institute of Technology, Pasadena 1936; 167.

[13] Vanoni AV. Sedimentation Engineering. Ed.: García MH. ASCE Manuals and Reports on Engineering Practice. ASCE; 2006.

[14] Singh V. Two dimensional sediment transport model using parallel computers (master's thesis). India: B.Tech., Banaras Hindu University; 2005.

[15] Yang CT. Sediment Transport: Theory and Practise, The McGraw-Hill Companies; 1996.

[16] DuBoys. Le Rhone et les Rivieres a Lit affouillable. Annales de Ponts et Chaussessec 1879; 5(18): 141-195.

[17] Straub LG. Missouri River Report. In-House Document 238, U.S. Government Printing Office; 1935.

[18] Meyer Peter E, Favre H, Einstein A. Neuere Versuchsresultate uber den Geschiebetrieb. Schweiz Bauzeitung 1934; 103 (13).

[19] Ackers P, White WR. Sediment transport: New approach and analysis. Journal of the Hydraulics Division, 1973; 99(Hy11) 2041-2060.

[20] Taylor EH. Flow characteristics at rectangular open-channel junctions. American Society of Civil Engineers1 1944; 70: 119–121.

[21] Webber NB, Greated CA. An investigation of flow behaviour at the junction of rectangular channels. Proceedings of Institute of Civil Engineers 1966; 34(3): 321–334.

[22] Yuan S, Xu L, Tang H, Xiao Y, Gualtieri C. The dynamics of river confluences and their effects on the ecology of aquatic enviremont: A review. Journal of Hydrodynamics 2022; 34: 1-14.

[23] Ashmore PE, Ferguson PI, Prestegaard KL, Ashworth PJ, Paola C. Secondary flow in anabranch confluences of a braided, gravel-bed stream. Earth Surface Processes and Landforms 1992; 17: 299-311.

[24] Roy AG, Roy R, Bergeron N. Hydraulic geometry and changes in flow velocity at a river confluence with coarse bed material. Earth Surface Processes and Landforms 1988; 13: 583-598.

[25] Ramamurthy AS, Carballada LB, Tran DM. Combining open channel flow at right angled junctions. Journal of Hydraulic Engineering 1988; 114(12).

[26] Rhoads BL. River Dynamics, online. Cambridge University Press; 2020.

[27] Wukkupondur A, Chandra V. Mittigate resorvoir sedimentation by reducing scour at river confluence: A exprerimental study. 8th International Perspective on Water Resorces and the Enviroment; 2016 Jan 4-6; Colombo, Sri Lanka.

[28] Joy DM., Townsend RD. Improved flow characteristics at a 900 channel confluence. Proceedings of the 5th Can. Hydrotechnical Conf, National Research Council Press, Ottawa 1981; 781–799.

[29] Best JL, Reid I. Separation zone at open-channel junctions. Journal of Hydraulic Engineering 1984; 110: 1588-1594.

[30] Schindfessel L, Creëlle S, De Mulder T. Flow patterns in an open channel confluence with increasingly dominant tributary inflow. Water 2015; 7: 4724-4751.

[31] Biron PM, Richer A, Kırkbride AD, Roy AG, Han S. Spatial patterns of water surface topography at a river confluence. Earth Surface Process and Landforms 2002;27:913-928.

[32] Best JL. Sediment transport and bed morphology at river channel confluences. Sedimentology 1988; 35:481-498.

[33] Best JL. Flow dynamics and sediment transport at river channel conjuences (doctoral thesis). London: Birkbeck College, University of London; 1985.

[34] Best JL, and Rhoads BL. Sediment transport, bed morphology and the sedimentology of river channel confluences. Ed.: Rice SP, Roy AG, Rhoads BL. River Confluences, Tributaries and the Fluvial Network. John Wiley and Sons Publishing; 2008. 45–72.

[35] Leite Ribeiro M., Blanckaert K, Roy, AG, Schleiss AJ. Flow and sediment dynamics in channel confluences. Journal of Geophysical Research 2012; 117 (F1), F01035.

[36] Baird DC, Fotherby L, Klumpp CC, Sculock SM. Bank Stabilization Design Guidelines, 2015.

[37] Klaassen GJ, Vermeer K. Confluence scour in large braided rivers with fine bed material. International Conference on Fluvial Hydraulics; 1988 January; Budapest.

[38] Biron P, Roy AG, Best JL. Bed morphology and sedimentology at the confluence of unequal depth channels. Geomorphology 1993; 8: 115-129.

[39] Ianniruberto M, Dantas E, Pinheiro A, Trevethan M, Filizola N, Santos A, et al. A field study of the confluence between Negro and Solimões Rivers Part 2: riverbed morphology and stratigraphy. Geoscience 2018; 350.

[40] Nazari-Giglou A, Jabbari-Sahebari A, Shakibaeinia A, Borgheid SM. An experimental study of sediment transport in channel confluences. International Journal of Sediment Research 2016; 31(1): 87-96.

[41] Borghei, SM, Sahebari AJ. Local scour at open-channel junctions. Journal of Hydraulic Research 2010; 48(4): 37-41.

[42] Zhang T, Feng M, Chen K. Hydrodynamic characteristics and channel morphodynamics at a large asymmetrical confluence with a high sediment-load main channel. Geomorphology 2020; 356.

[43] Rhoads BL, Sukhodolov AN. Spatial and temporal structure of shear-layer turbulence at a stream confluence. Water Resources Research 2004; 40: 1–13.

[44] Shakibaeinia A, Zarrati AR, Tabatabai MRM. Three-dimensional numerical study of river channel confluence with bed changes. Proceeding of 32nd IAHR Congress; 2007; Venice,Italy. 32(2): 609–617.

[45] Shakibaeinia A, Tabatabai MRM, Zarrati AR. Reply to the discussion on three-dimensional numerical study of flow structure in channel confluences. Canadian Journal of Civil Engineering 2011; 38(1): 127–129.

[46] Yu Q, Yuan S, Rennie CD. Experiments on the morphodynamics of open channel confluences: implications for the accumulation of contaminated sediments. JGR Earth Surface 2020; 125(9).

[47] Balouchi B, Shafai-Bejestan M, Ruther N, Rahmanshahi M. Experimental investigation of flow pattern over a fully developed bed at a 60° river confluence in large floods. Acta Geophysica 2022; 70: 2283-2296.

Curriculum Vitae

Personel Information:

Name Surname : Zehra Büyüker

Nationality : Turkish (TC)

Education:

Degree	**Institution**
B. Sc.	Ege University, Department of Civil Engineering (2012–2017)
M. Sc.	Ege University, Department of Civil Engineering (Structural Engineering) (2017–2019)

Work Experience:

Year	**Place**
Feb. 2021 -	Izmir Kâtip Celebi University (Lecturer)
Oct. 2022 - Dec. 2022	Instituto Superior Tecnico (IST) (Resarcher)
Apr. 2018 - Feb. 2021	Hamaş Endüstri A.Ş (Civil Engineer)

Conference Paper:

Öztürk B, **Büyüker Z**, Taşkaya E, Bombar G, Cardoso AH. Simetrik Akarsu Kavşağında Zamanın Taban Morfolojisine Etkisi. XI. Ulusal Hidroloji Kongresi, 13-14 October 2022, Gaziantep University,Gaziantep, Türkiye (full paper).